Journal of Geointerface, Vol. 4, No. 2, December 2025, pp. 182–206 e-ISSN: 2583-6900

Geochemistry and chemical (Th–U–Pb) monazite age of Pamuru Granite interface of Nellore Schist Belt and Nallamalai Fold Belt, Southern India: Implication for Columbia Break up and Pan-African assembly

Mrunalini V. Khond [1,*], Tushar Meshram [2], Tarun Koley[3], Mahima M.[3]

[1] *National Mission -II, Geological Survey of India, Central Region, Nagpur, India*
[2] *Geological Survey of India, Central Region, Nagpur, India*
[3] *State Unit Andhra Pradesh, Geological Survey of India, Southern Region, Hyderabad, India*

ABSTRACT

The Proterozoic granitic magmatism along the interface of the Nallamalai Fold Belt (NFB) and the adjoining Nellore Schist Belt (NSB) in southern India exhibits a distinct arc-back arc tectonic setting. The granites emplaced along the interface of Cuddapah/ NFB and NSB exhibited distinct geochemical traits and geochronological ages ie., granites (e.g. Vinukonda) with age ∼1575 Ma display an arc-magmatic signature, while other granites (e.g. Kanigiri) show age of 1240 Ma with rift-related petrogenetic signature indicative of an extensional arc setting. This study presents a detailed petrogenetic analysis of the Pamuru granite (PG) and reports chemical Th–U–Pb monazite ages situated along the Terrain Boundary Tectonic Zone (TBTZ) along NSB and Cuddapah Basin. The PG predominantly consist of plagioclase feldspar, K-feldspar, and quartz, along with biotite and muscovite. It also hosts accessory minerals such as allanite, zircon, monazite, epidote, garnet and sphene. Geochemically, PG exhibits high calc-alkaline to shoshonitic affinity, a compositional trend ranging from peralkaline to peraluminous, and is typically ferroan in nature. These granites plot within the post-collisional to late-orogenic tectonic fields, suggesting emplacement in a within-plate setting. The trace element signatures of PG highlight the role of highly differentiated magma and indicate significant contribution from the lower crust in the evolution of this A_2-type granite. Th–U–Pb chemical dating of rounded, zoned monazite grains from PG reveals two distinct age populations: 1651 ± 58 Ma and 513 ± 50 Ma, corresponding to the well-differentiated cores (ThO_2:avg. 6.61–13.82 wt.%) and rims (ThO_2:avg. 7.25–8.58 wt.%), respectively. Textural evidence and previously reported age data suggest that these monazites are xenocrystic in nature, likely derived from the 1615 ± 25 Ma to 1589 ± 5.7 Ma analogous granitic magma. However, PG geochemical characteristics exhibit a contrasting nature with VIN granites (1615 Ma). But, it shows similar geochemical signatures akin to TBTZ granite (1284 Ma). The upper intercept ages (1681 ± 55 Ma and 1567 ± 73 Ma) represent magmatic emplacement events, consistent with the final assembly of the Columbia supercontinent (1.8 to 1.6 Ga). In contrast, the lower intercept ages (511 ± 47 Ma and 515 ± 53 Ma) recorded in the monazite rims reflect a Pan-African thermal overprint on the PG. These ages represent the Pan-African incorporation of India into the Gondwana supercontinent.

ARTICLE HISTORY

Received: 13 Aug 2025
Revised: 16 Oct 2025
Accepted: 17 Oct 2025

https://doi.org/10.5281/zenodo.17435017

KEYWORDS

Pamuru Granite
(Th–U–Pb) monazite age
Nellore Schist belt
Nallamalai Fold Belt
Gondwana supercontinent

*Corresponding author. Email: mvkhond@gmail.com (MV), tusharmeshram2911@gmail.com (TM), tarun.koley72@gmail.com (TK), mahima737@gmail.com (MM)

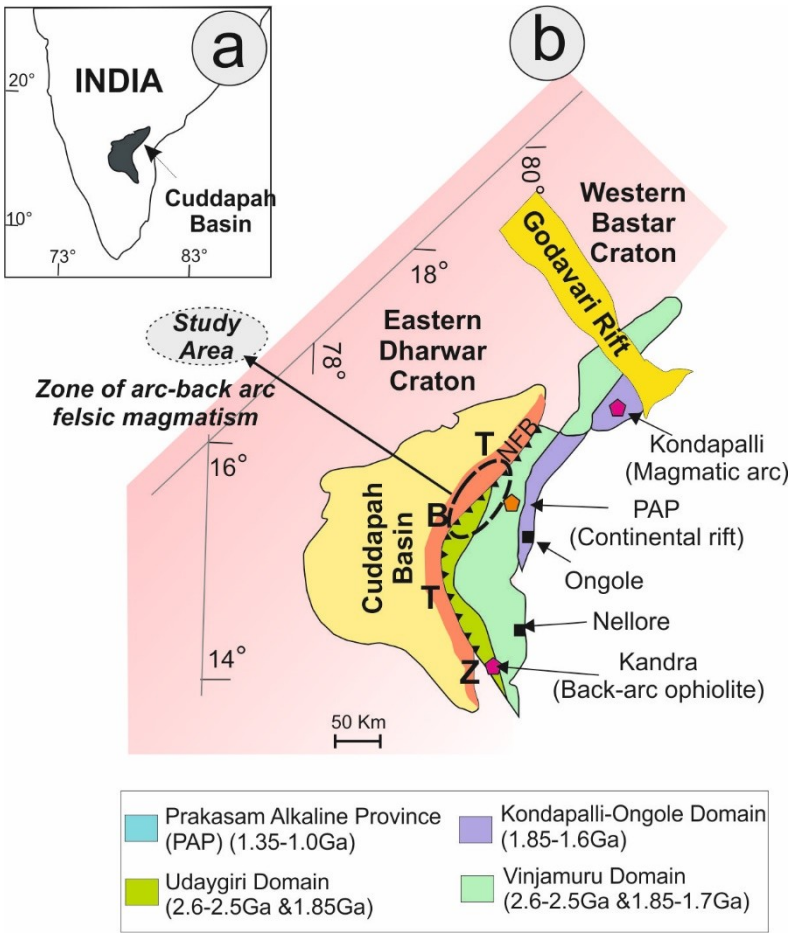

Fig. 1. a) Inset map shows a diagrammatic representation of the Cuddpah Basin (GIPFOB; modified after Radhakrishna and Naqvi, 1986) b) Generalized geological map of the EGGB with four distinct crustal provinces with TBTZ (Terrain Boundary Tectonic Zone) (modified after Dobmeier and Raith, 2003). Note that the Mesoproterozoic rift magmatism is present between the Vinjamuru and Ongole domains of the Krishna Province (Vijaya Kumar et al., 2011). The circle marked study area indicates Paleoproterozoic felsic arc back-arc magmatic zone.

1. Introduction

The Eastern Dharwar Craton (EDC) of southern India forms part of the Archean Dharwar Craton, is primarily composed of Neoarchean granitoids (2.7–2.51 Ga) and narrow greenstone belts, along with granulite facies rocks (~2.52–2.51 Ga), reflecting high-grade metamorphism and deep crustal processes (Swaminath et al., 1976; Chadwick et al., 2000; Jayananda et al., 2006; Peucat et al., 2013; Meshram et al., 2021). The eastern margin of the EDC is bounded by the Proterozoic Cuddapah Basin and the NSB, separated by the Terrain Boundary Tectonic Zone (TBTZ), as a major crustal scale tectonic zone (Chetty and Murthy, 1994). This zone records multiple Proterozoic tectono-magmatic events, including subduction, arc magmatism, and back-arc extension, reflected in ophiolites, anorthosites, and extensive granitic intrusions from ~1.8 to 1.2 Ga (Saha et al., 2018; Meshram et al., 2022; Sesha Sai, 2023).

These magmatic episodes are closely linked to the assembly and breakup of the Columbia supercontinent (1.8–1.3 Ga), with southern India likely forming part of its active continental margin (Rogers and Santosh, 2002; Zhao et al., 2011).

The interface of the NSB and the NFB part of the Cuddapah Basin marked as a regional tectonic zone known as the TBTZ. The extensive Paleoproterozoic feldspathic magmatism is commonly noticed along the TBTZ extending from Sri Kalahasti in the south to Podili to the north. They are further divided into two groups namely VIN granites and TBTZ granites with respect to distinct tectono-magmatic characteristics. The emplacement of the VIN granites along the TBTZ reflects arc magmatism during the Mesoproterozoic, marking crustal accretion processes linked to the Rodinia supercontinent assembly (Sesha Sai, 2023). The ~1.5 Ga, Venukonda granite is

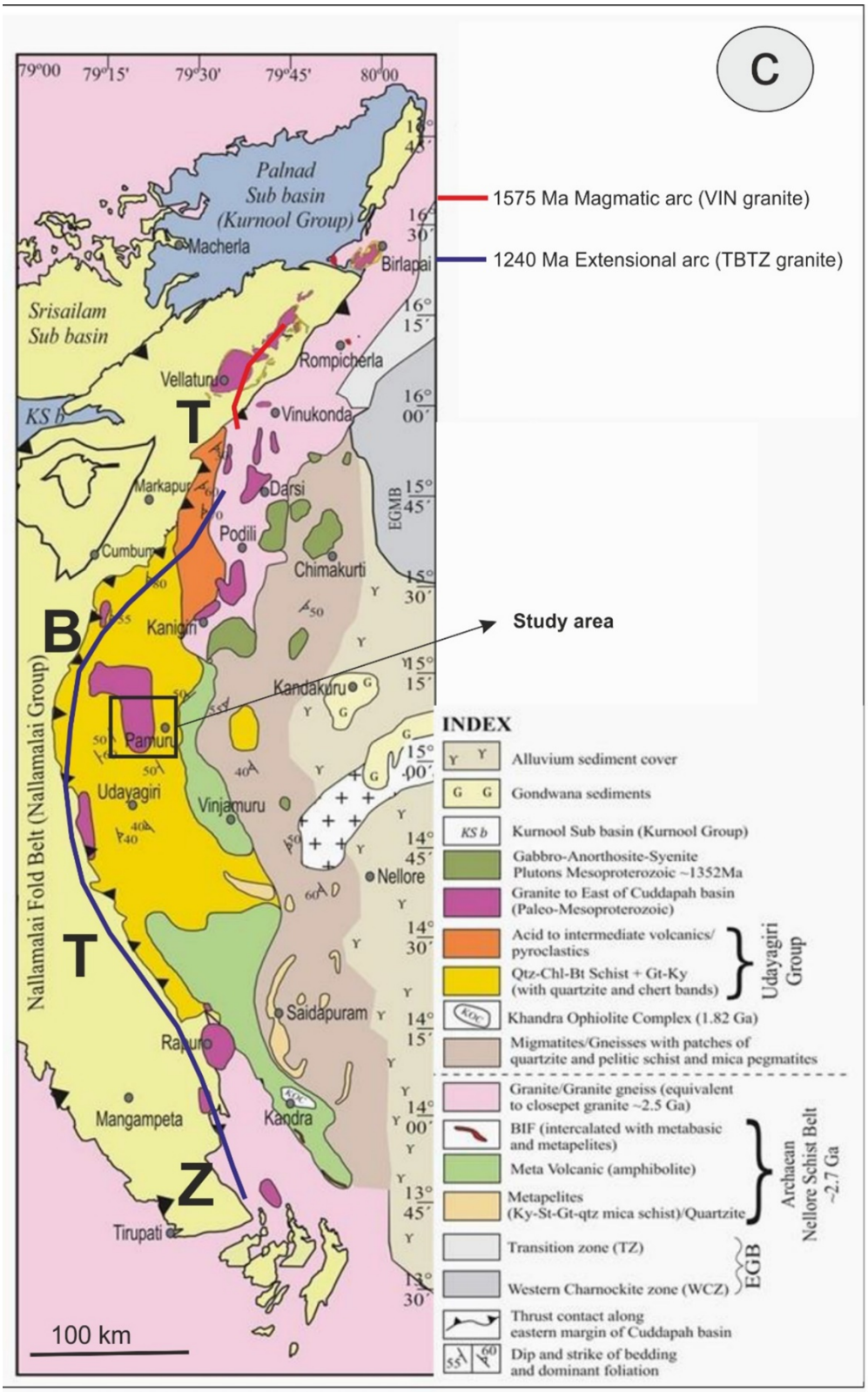

Fig. 1. c) Geological Map of the area adjoining NFB and NSB eastern Dharwar Craton, Southern India (after GSI, 1981; Nagaraja Rao et al., 1987; Srinivasan et al., 1994)

part of VIN granites and situated close to the eastern margin of Vellaturu granite (Dobmeier et al., 2006, Gupta et al., 1984). In contrast, younger TBTZ granites (~1.2 Ga, Kanigiri granite, Gupta et al., 1984;

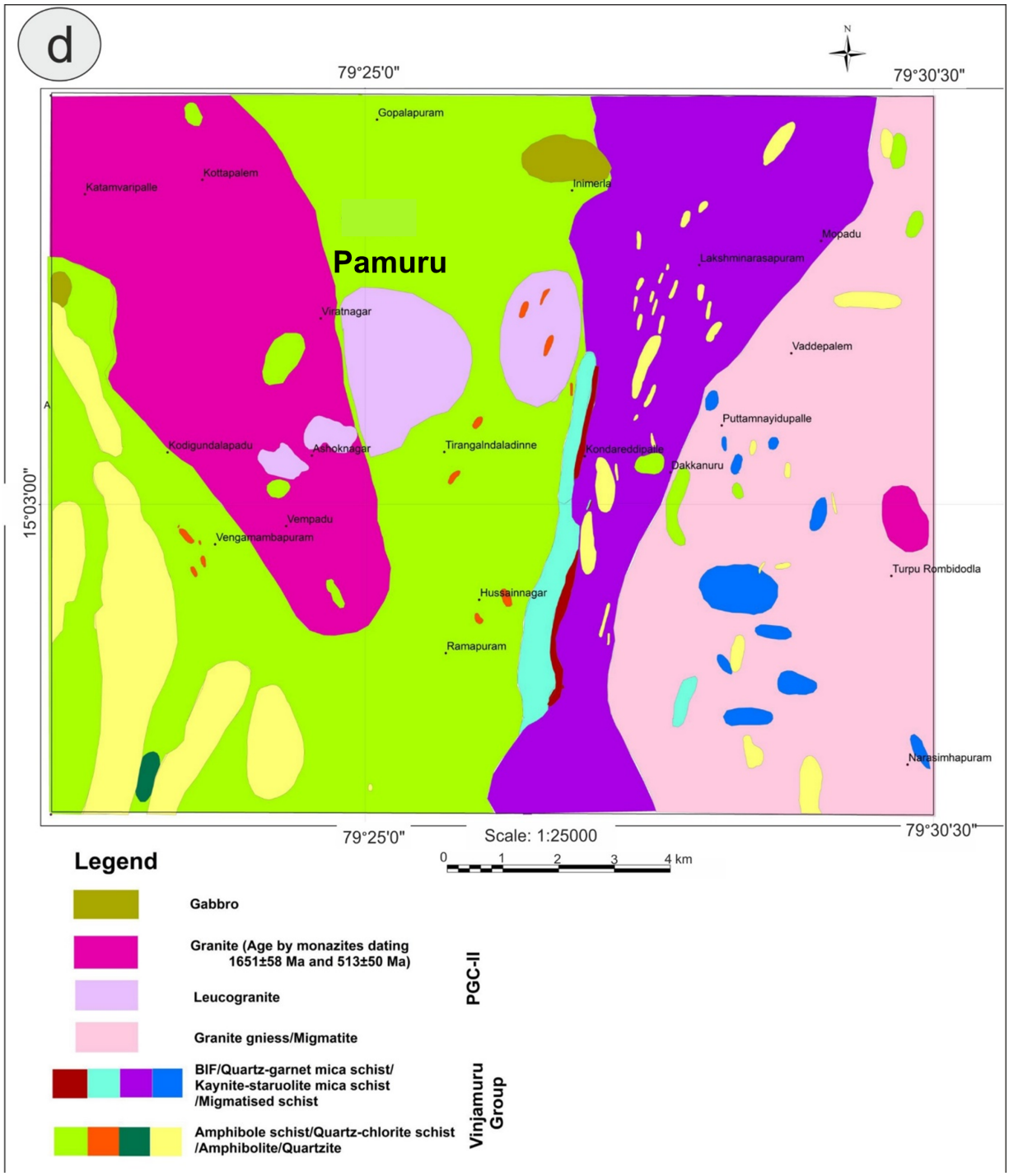

Fig. 1. d) Geological map of the study area shows the location of Pamuru granite within NSB and Eastern Dharwar gneisses

Dharma Rao and Santosh, 2011) and alkaline rocks of the Prakasam Province record extensional, back-arc magmatism. The TBTZ granites, including those at Pamuru, Srikalahasti, Rapuru, and Kanigiri, are aligned along a ~350 km curvilinear belt along the western margin of the NSB, indicating a prolonged and spatially extensive Mesoproterozoic magmatic episode (Sesha Sai, 2013, 2023; Narshimha et al., 2022). In particular, the VIN (~1575 Ma) and TBTZ (~1240 Ma) granites reflect early arc and later extensional tectonic settings, respectively, as key indicators of crustal growth and supercontinent reconstruction (Sain and Saha, 2018; Narshimha et al., 2022). Furthermore, the geodynamic settings of these granites provide critical insights into tectono-magmatic processes operating along ancient plate margins.

The Pamuru granite, intruded within the TBTZ near the western margin of the Nellore Schist Belt, provides an opportunity to understand Proterozoic crustal evolution in southern India. Despite its tectonic and petrogenetic significance, detailed geochemical and geochronological studies on this granite are limited. This study aims to fill that gap by investigating the petrogenesis of the Pamuru granite pluton, using integrated geochemical analyses and monazite (Th–U–Pb) age dating, to reconstruct its tectonic setting and assess its implications in the broader framework of the Columbia supercontinent breakup and subsequent Pan-African connections.

2. Geological Setting

Dharwar craton is largest craton in the southern part of Peninsular India. It is subdivided into two distinct crustal terranes, the Western Dharwar Craton (WDC) and the Eastern Dharwar Craton (EDC), and limited by the Chitradurga shear zone and ~2.5 Ga Closepet Granite intrusion (Jayananda et al., 2000; Moyen et al., 2003). The WDC is composed of basement migmatite tonalitic gneisses known collectively as the Peninsular Gneiss, older Sargur Group and greenstone belts i.e, (Jayananda et al., 2000; Meen et al., 1992; Peucat et al., 1993; Hokada et al., 2013). The EDC is made up dominantly of young (ca. 2.70–2.53 Ga) crust including gneisses, TTGs, syn to late-kinematic High-Mg diorites or sanukitoids and calc-alkaline-K-rich granites (Jayananda et al., 2000; Chardon and Jayananda, 2008; Mukherjee et al., 2017) with the interleaving of ~2.70 Ga narrow greenstone belts (Chadwick et al., 2000; Jayananda et al., 2000). The NSB is situated extremely east of EDC and shares its contact with the Proterozoic Cuddapah Basin (~1.7 Ga) (Fig. 1a) and NFB marked by the TBTZ (Chetty and Murthy, 1994; Chetty, 2011; Chetty, 2017) with an emplacement of subduction-related arc-back-arc as well as rift-related Proterozoic felsic, alkaline and mafic magmatism (Fig. 1b) (Sesha Sai, 2013, 2023). These terrain boundaries have tectonically distinct events of Proterozoic granite magmatism demarcated in the form of VIN granites along the NE fringes of NFB and TBTZ granites along the western margin of NSB (Sesha Sai, 2013, 2019, 2023).

The VIN (~1.5 Ga; Vellaturu-Ipuru-Nakerikallu) arc magmatic granites restricted along an NNE-SSW emplacement axis in the northeastern fringes of the NFB and represent an important zone of magnesian feldspathic magmatism in the southeastern part of peninsular India (Sesha Sai, 2019). They are emplaced close to the vicinity of the TBTZ i.e. at the interface of the Proterozoic Nallamalai orogenic belt and adjoining Precambrian amphibolite gneissic accretionary terrain in the northern part of NSB (Sesha Sai, 2019; Hazra et al., 2004). In contrast, the TBTZ granitoids (~1.2 Ga; Vinukonda, Kanigiri, Darsi, Pamuru, Rapuru, Srikalahasti) of NSB are sporadically exposed close along the eastern margin of NFB. These Mesoproterozoic felsic intrusive occur from Vinukonda in North to South of Rapur and show a curvilinear emplacement zone of more than 350 km along the western margin of NSB (Sesha Sai, 2013, 2023).

3. Field and Petrographic study

The Pamaru granite pluton is mainly intruded within the metasedimentary rocks of NSB and also extends to the areas i.e., Komatigunta, Eguvapalle, and Chandrashekarapuram western margin of NSB (Fig. 1c–d).

The PG generally 150 Sq. km elongated body occurs near the Anumalakonda and Pamuru village intruded in the metasedimentary units of the Nellore Schist belt. The PG is dominantly massive at the central part of the pluton, whereas, it is foliated in nature along the margin of pluton. A few small xenoliths of the NSB and older granites were also observed at places. They are leucocratic in nature and shows presence of biotite as major mafic phase. The biotite shows the development of crude foliation plan along the pluton margins and defines the foliation in the rock (Fig. 2a–f). The feldspars are medium-grained and shows common association with quartz. The biotite at places shows the alteration into chlorite. Although the Garnet insignificant in the Pamuru granite, but it is observed at places in field as well as in petrographic section as an accessory. The garnets are generally developed along contact of granite and meta-sedimentary rocks of NSB. Hence, they may be contact metasomatic in nature, not represented as a part of metasomatism. At places it contains pyrite as accessory phase. Late hydrothermal activity is represented by white quartz veins and pegmatite veins.

Petrographically, PG is medium to coarse grained, shows holocrystalline texture and is mainly composed of quartz, microcline, plagioclase, muscovite, biotite

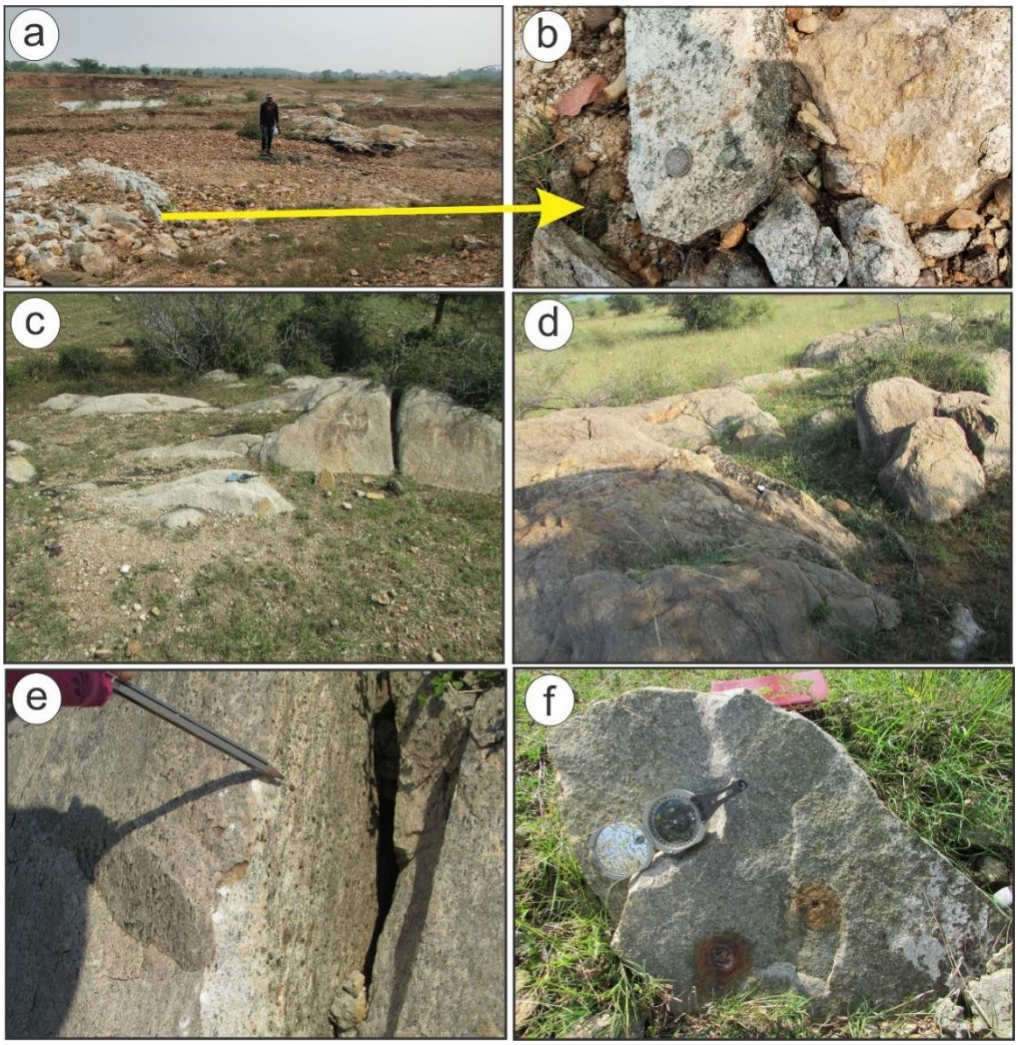

Fig. 2. Field photographs of a) Pamuru granite show ground level outcrop pattern. b) Close view of Pamuru granite show leucocratic nature with the presence of mafic minerals specially biotite. c) Pamuru granite with E–W joints d) Field photographs of Alkali rich granite e) Pamuru granite showing magnetite f) Massive granite north of Kondareddipalle village.

and chlorite with accessory epidote, garnet, titanite and opaques (Fig. 3). Quartz occurs as a subhedral grain dominating after the feldspar shows typical undulating extinction. Quartz grains show development of microstructure with boundary migration and recrystallization as a result of deformation. K-feldspar is dominating over the plagioclase feldspar. The tartan twinning is very common in K-feldspar whereas, plagioclase shows polysynthetic twining (Fig. 3a). The microstructure development in feldspars exhibited by sub grain formation and untwined nature. The development of myrmekite texture between quartz and K-feldspar observed at places (Fig. 3a). Biotite and muscovite occur as interstitial to the feldspar and quartz (Fig. 3b–c). At places, these grains are deformed in nature showing recrystallized grain boundaries. Biotite shows brown pleochroism, common association with muscovite and garnet at places. Garnets are euhedral to subhedral in shape at places fractured in nature (Fig. 3c). It contains monazite, allanite and zircon as discrete grains occurring as an inclusion or along grain boundaries or fractures as an accessory phase (Fig. 3d–e–f). Likewise, magnetite, ilmenite and pyrite also occur in minor amounts.

4. Methodology

Samples were collected from Pamuru granites and prepared thin cum polished section for further studies. The petrographic observations were done under the Lieca DM 2700P Microscope at the Regional Petrology Laboratory, GSI, SR, Hyderabad, India. The major element compositions of different mineral

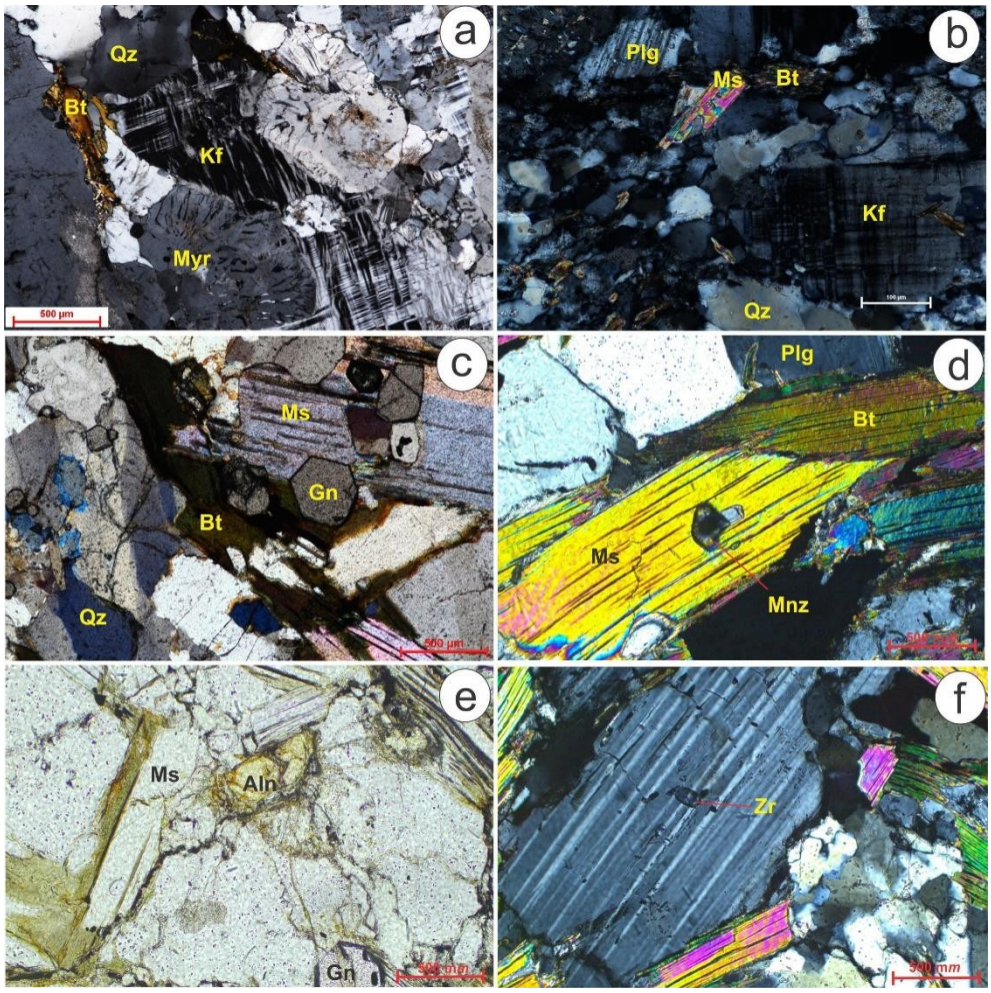

Fig. 3. Photomicrographs showing textural and mineralogical variations in Pamuru granite. a) The presence of k-feldspar with the development of myrmekite texture along the contact with quartz, biotite occurs as an interstitial phase. b) The muscovite is in an interstitial phase to the k-feldspar and plagioclase feldspar. c) The presence of euhedral garnets associated with muscovite and biotite occurs as an interstitial phase. d) The monazite occurs as inclusion within muscovite in association with biotite. e) The presence of zoned allanite shows the development of radial crack. f) The presence of tiny zircon inclusion occurs as inclusion within plagioclase.

phases were measured on a Cameca SX-100 Electron Probe Micro Analyser (EPMA) at the Petrology and EPMA Lab, Hyderabad, India. The operating conditions were 15 kV accelerating voltage, 15 nA beam current, beam size 1 m with the peak, and the background time are 10 s and 5 s, respectively. Instrument calibration was done by using natural and synthetic mineral standards. ZAF correction of Pouchou and Pichoir (1984) was used for matrix correction. The processed data are listed in Table 1 and 3. supplementary files.

A total of eighteen of fresh samples from PG were chosen for analyses of whole-rock major and trace element concentrations. The major elements (reported as wt% oxide) with few trace elements were measured on a PANalytical Magix 2424 XRF. The rare earth elements (REE) and other trace element concentrations were determined on an Elan DRC-e Perkin Elmer SCIEX, AH16901006 Inductively Coupled-Plasma Mass Spectrometer (ICP-MS) at Chemical Division, GSI, SR, Hyderabad. The precision and accuracy of analyses were double-checked by repeated analyses of international reference standards (http://www.gsiportal.gov). The whole rock, trace element and rare earth element data are listed in Tables 4, 5 and 6.

The EPMA analysis of monazite grain has been carried out at EPMA Laboratory, Geological Survey of India, Southern Region, Hyderabad. EPMA, utilizing instruments like CAMECA SX-100, is used to determine the elemental composition of monazite, including rare earth elements (REEs), thorium (Th),

e-ISSN: 2583-6900

Table 1. EPMA of the feldspars from Parumru granite.

	K- feld	K- feld	K- feld	K- feld	K- feld	K- feld	K- feld	K- feld	K- feld	K- feld	K- feld	K- feld	Plagi	Plagi	Plagi	Plagi	Plagi	Plagi
Pt	133 / 1 .	134 / 1 .	137 / 1 .	138 / 1 .	36 / 1 .	37 / 1 .	38 / 1 .	39 / 1 .	40 / 1 .	64 / 1 .	65 / 1 .	75 / 1 .	64 / 1 .	65 / 1 .	66 / 1 .	67 / 1 .	71 / 1 .	15 / 1 .
SiO_2	65.00	64.70	64.71	65.30	65.11	64.53	64.58	64.14	64.79	64.363	63.40	63.91	58.18	58.53	59.11	59.05	58.66	59.96
TiO_2	0.00	0.00	0.00	0.00	0.00	0.01	0.06	0.00	0.00	0	0.00	0.02	0.00	0.03	0.00	0.02	0.00	0.00
Al2O3	18.01	18.12	18.01	17.66	18.21	17.72	18.20	17.86	17.81	18.318	17.76	17.84	25.96	25.63	26.18	25.67	25.93	26.51
Cr2O3	0.00	0.00	0.00	0.00	0.00	0.00	0.00	0.00	0.00	0.00	0.00	0.00	0.00	0.00	0.00	0.00	0.00	0.00
Fe2O3	0.00	0.00	0.00	0.00	0.00	0.00	0.00	0.00	0.00	0	0.00	0.00	0.00	0.00	0.00	0.00	0.00	0.01
FeO	0.05	0.00	0.00	0.11	0.15	0.07	0.04	0.00	0.09	0	0.00	0.00	0.13	0.05	0.02	0.11	0.08	0.02
MnO	0.01	0.00	0.03	0.05	0.04	0.00	0.02	0.00	0.08	0	0.01	0.00	0.01	0.02	0.00	0.00	0.01	0.05
MgO	0.00	0.00	0.00	0.01	0.00	0.00	0.00	0.00	0.00	0.052	0.05	0.00	0.00	0.00	0.00	0.00	0.00	0.00
CaO	0.00	0.00	0.00	0.00	0.00	0.00	0.00	0.00	0.00	0	0.00	0.04	7.18	7.48	7.65	7.31	7.47	7.69
BaO	0.00	0.00	0.00	0.00	0.00	0.00	0.00	0.00	0.00	0.00	0.00	0.00	0.00	0.00	0.00	0.00	0.00	0.00
Na2O	0.87	0.63	1.10	0.66	0.83	0.85	0.78	0.81	0.72	0.847	0.46	0.49	7.53	7.39	7.27	7.44	7.24	6.94
K2O	15.96	16.19	15.20	16.04	15.13	14.89	15.56	15.21	15.43	15.943	16.13	16.27	0.04	0.08	0.06	0.05	0.05	0.10
Total	99.91	99.64	99.05	99.82	99.47	98.06	99.23	98.00	98.91	99.52	97.80	98.57	99.18	99.29	100.44	99.56	99.50	99.41
Cation	8(O)																	
Ab	7.7	5.6	9.9	5.9	7.7	7.9	7.1	7.5	6.6	7.5	4.10	4.40	0.23	0.45	0.34	0.29	0.30	0.56
An	0	0	0	0	0	0	0	0	0	0	0.00	0.20	65.35	63.85	63.01	64.64	63.48	61.67
Or	92.3	94.4	90.1	94.1	92.3	92.1	92.9	92.5	93.4	92.5	95.90	95.40	34.42	35.69	36.64	35.07	36.22	37.77
Ab+An	7.7	5.6	9.9	5.9	7.7	7.9	7.1	7.5	6.6	7.5	4.10	4.60	100.00	100.00	100.00	100.00	100.00	100.00
Si	2.925	2.997	3.010	3.023	3.025	3.041	3.004	3.021	3.028	2.979	2.994	2.995	2.615	2.630	2.631	2.643	2.632	2.637
Ti	0.000	0.000	0.000	0.000	0.000	0.000	0.002	0.000	0.000	0.000	0.000	0.001	0.000	0.001	0.000	0.001	0.000	0.000
Al	0.955	0.989	0.987	0.964	0.997	0.984	0.998	0.991	0.981	0.999	0.988	0.985	1.375	1.358	1.373	1.354	1.371	1.374
Cr	0.000	0.000	0.000	0.000	0.000	0.000	0.000	0.000	0.000	0.000	0.000	0.000	0.000	0.000	0.000	0.000	0.000	0.000
Fe3	0.002	0.000	0.000	0.000	0.000	0.000	0.000	0.000	0.000	0.000	0.000	0.000	0.005	0.002	0.000	0.004	0.000	0.000
Fe2	0.000	0.000	0.000	0.004	0.006	0.003	0.002	0.000	0.003	0.000	0.000	0.000	0.000	0.000	0.001	0.000	0.003	0.001
Mn	0.000	0.000	0.001	0.002	0.001	0.000	0.001	0.000	0.003	0.000	0.000	0.000	0.000	0.001	0.000	0.000	0.000	0.002
Mg	0.000	0.000	0.000	0.001	0.000	0.000	0.000	0.000	0.000	0.004	0.003	0.000	0.000	0.000	0.000	0.000	0.000	0.000
Ca	0.000	0.000	0.000	0.000	0.000	0.000	0.000	0.000	0.000	0.000	0.000	0.002	0.346	0.360	0.365	0.350	0.359	0.363
Ba	0.015	0.000	0.000	0.000	0.000	0.000	0.000	0.000	0.000	0.000	0.000	0.000	0.000	0.000	0.000	0.000	0.000	0.000
Na	1.393	0.057	0.099	0.059	0.074	0.077	0.070	0.074	0.065	0.076	0.042	0.045	0.656	0.644	0.627	0.646	0.629	0.592
K	0.006	0.957	0.902	0.947	0.897	0.895	0.924	0.914	0.920	0.942	0.972	0.973	0.002	0.005	0.003	0.003	0.003	0.005

Table 2. EPMA of mica from Pamuru Granite.

	3 / 1 .	4 / 1 .	7 / 1 .	8 / 1 .	16 / 1 .	17 / 1 .	21 / 1 .	22 / 1 .	25 / 1 .	27 / 1 .	30 / 1 .	31 / 1 .	18 / 1 .	26 / 1 .
	Mus										Biotite			
SiO_2	46.38	47.49	48.30	47.98	46.98	46.56	47.21	48.22	47.66	47.58	39.59	39.964	38.84	39.85
TiO_2	0.29	0.39	0.24	0.29	0.27	0.36	0.24	0.31	0.49	0.30	0.50	1.05	1.20	1.16
Al_2O_3	34.52	33.56	35.19	34.15	33.89	34.49	35.14	34.76	33.90	34.88	18.62	18.965	18.54	19.10
Cr_2O_3	0.00	0.06	0.02	0.02	0.05	0.00	0.02	0.03	0.02	0.00	0.00	0	0.02	0.00
FeO^T	2.96	3.07	2.55	2.46	2.72	2.88	2.41	2.46	2.96	3.10	12.84	12.261	11.63	11.35
MnO	0.05	0.00	0.00	0.07	0.02	0.06	0.04	0.00	0.07	0.00	0.22	0.053	0.11	0.22
MgO	0.92	0.96	0.88	0.89	0.94	0.90	0.90	0.87	0.94	0.96	15.41	15.341	16.06	15.96
CaO	0.00	0.00	0.00	0.03	0.00	0.00	0.01	0.00	0.00	0.00	0.10	0	0.16	0.29
Na_2O	0.71	0.95	0.59	0.95	0.90	0.67	0.70	0.88	0.78	0.88	0.19	0.199	0.27	0.18
K_2O	9.43	7.76	9.59	7.45	7.99	9.37	9.78	7.58	8.34	9.94	8.55	9.088	8.19	7.68
NiO	0.00	0.00	0.05	0.00	0.00	0.01	0.00	0.02	0.00	0.01	0.11	0.032	0.00	0.00
Total	95.29	94.24	97.42	94.28	93.76	95.30	96.44	95.13	95.17	97.64	96.13	96.954	95.02	95.79
Fe_2O_3	0.00	0.00	0.00	0.00	0.00	0.00	0.00	0.00	0.00	0.00	0.00	0	0.00	0.00
FeO	2.96	3.07	2.55	2.46	2.72	2.88	2.41	2.46	2.96	3.10	12.84	12.261	11.63	11.35
Total	95.26	94.23	97.42	94.28	93.77	95.30	96.44	95.13	95.17	97.64	96.13	96.953	95.02	95.77
Cations :	22(O)	22(O)	22(O)	22(O)	22(O)	22(O)	22(O)	22(O)	22(O)	22(O)	22(O)	22(O)	22(O)	22(O)
Si	6.19	6.34	6.27	6.36	6.30	6.21	6.21	6.33	6.31	6.21	5.71	5.70	5.63	5.69
Ti	0.03	0.04	0.02	0.03	0.03	0.04	0.02	0.03	0.05	0.03	0.05	0.11	0.13	0.12
Al	5.43	5.28	5.39	5.34	5.36	5.42	5.45	5.38	5.29	5.37	3.16	3.19	3.17	3.21
Cr	0.00	0.01	0.00	0.00	0.01	0.00	0.00	0.00	0.00	0.00	0.00	0.00	0.00	0.00
Fe^{+3}	0.00	0.00	0.00	0.00	0.00	0.00	0.00	0.00	0.00	0.00	0.00	0.00	0.00	0.00
Fe^{+2}	0.33	0.34	0.28	0.27	0.31	0.32	0.26	0.27	0.33	0.34	1.55	1.46	1.41	1.35
Mn	0.01	0.00	0.00	0.01	0.00	0.01	0.00	0.00	0.01	0.00	0.03	0.01	0.01	0.03
Mg	0.18	0.19	0.17	0.18	0.19	0.18	0.18	0.17	0.19	0.19	3.31	3.26	3.47	3.40
Ca	0.00	0.00	0.00	0.00	0.00	0.00	0.00	0.00	0.00	0.00	0.02	0.00	0.02	0.04
Na	0.18	0.25	0.15	0.24	0.23	0.17	0.18	0.22	0.20	0.22	0.05	0.06	0.07	0.05
K	1.61	1.32	1.59	1.26	1.37	1.59	1.64	1.27	1.41	1.66	1.57	1.65	1.52	1.40
Ni	0.00	0.00	0.01	0.00	0.00	0.00	0.00	0.00	0.00	0.00	0.01	0.00	0.00	0.00
Total	13.96	13.76	13.88	13.69	13.79	13.93	13.95	13.69	13.79	14.01	15.47	15.45	15.45	15.30
Fe T	0.33	0.34	0.28	0.27	0.31	0.32	0.26	0.27	0.33	0.34	1.55	1.46	1.41	1.35

Table 3. EPMA of garnet from Pamuru granite.

	32 / 1 .	33 / 1 .	36 / 1 .	39 / 1 .	41 / 1 .	48 / 1 .	54 / 1 .	55 / 1 .	58 / 1 .	61 / 1 .	62 / 1 .	1 / 1 .	2 / 1 .	5 / 1 .	6 / 1 .	12 / 1 .	19 / 1 .	20 / 1 .	28 / 1 .	29 / 1 .
SiO_2	35.91	37.77	37.21	36.63	36.34	36.45	38.10	38.37	36.82	37.14	37.28	37.79	38.06	36.55	38.48	36.84	38.22	36.69	38.13	38.66
TiO_2	0.00	0.01	0.00	0.00	0.00	0.02	0.00	0.06	0.00	0.02	0.00	0.05	0.05	0.00	0.03	0.00	0.01	0.00	0.01	0.00
Al_2O_3	21.86	22.02	21.88	21.50	21.48	21.91	21.99	21.83	21.48	21.72	21.06	21.34	21.99	21.78	21.79	21.66	21.44	21.80	21.80	21.60
Cr_2O_3	0.00	0.00	0.00	0.00	0.00	0.00	0.00	0.00	0.03	0.00	0.01	0.06	0.04	0.01	0.03	0.00	0.00	0.00	0.00	0.00
FeO^T	28.31	29.22	28.66	29.49	28.77	28.18	27.82	28.04	27.88	28.81	28.67	24.97	25.44	25.01	24.21	24.48	24.99	24.61	24.83	25.31
MnO	6.38	6.56	6.72	6.24	6.41	7.34	6.69	6.05	6.27	6.10	6.14	9.28	9.13	9.31	9.24	9.01	9.19	8.98	9.64	9.50
MgO	4.15	3.71	4.04	3.91	3.70	4.13	4.14	3.68	3.73	4.02	3.63	4.33	4.09	3.72	3.78	4.31	4.49	3.92	4.06	3.91
CaO	2.61	2.66	2.70	2.52	2.68	2.41	2.51	3.09	2.81	2.56	2.72	2.67	2.66	3.18	3.08	2.60	2.63	2.67	2.39	2.64
Na_2O	0.00	0.00	0.00	0.00	0.05	0.00	0.04	0.00	0.07	0.00	0.01	0.00	0.00	0.01	0.03	0.03	0.03	0.01	0.00	0.02
K_2O	0.00	0.00	0.00	0.00	0.00	0.00	0.00	0.01	0.01	0.00	0.02	0.00	0.00	0.00	0.04	0.00	0.02	0.02	0.04	0.02
NiO	0.00	0.00	0.00	0.03	0.00	0.01	0.00	0.00	0.09	0.00	0.00	0.05	0.00	0.00	0.00	0.00	0.00	0.00	0.00	0.00
Total	99.21	101.96	101.21	100.31	99.44	100.44	101.27	101.14	99.20	100.36	99.54	100.44	101.46	99.56	100.70	98.92	101.03	98.70	100.89	101.67
Fe_2O_3	2.86	0.79	1.82	2.48	2.34	2.73	0.00	0.00	1.03	1.11	0.42	0.37	0.00	1.66	0.00	0.75	0.18	0.37	0.00	0.00
FeO	25.74	28.51	27.02	27.26	26.67	25.73	27.82	28.04	26.96	27.81	28.29	24.64	25.44	23.52	24.21	23.80	24.83	24.28	24.83	25.31
Total	99.49	102.03	101.39	100.56	99.67	100.72	101.27	101.13	99.30	100.47	99.58	100.57	101.46	99.73	100.70	99.00	101.04	98.73	100.89	101.67
Cations:	12(O)	12(O)	12(O)	12(O)	12(O)	12(O)	12(O)	12(O)	12(O)	12(O)	12(O)	12(O)	12(O)	12(O)	12(O)	12(O)	12(O)	12(O)	12(O)	12(O)
Si	2.88	2.96	2.93	2.92	2.92	2.89	2.99	3.01	2.96	2.95	2.99	2.99	2.98	2.92	3.03	2.96	3.00	2.96	3.00	3.02
Ti	0.00	0.00	0.00	0.00	0.00	0.00	0.00	0.00	0.00	0.00	0.00	0.00	0.00	0.00	0.00	0.00	0.00	0.00	0.00	0.00
Al	2.07	2.03	2.03	2.02	2.03	2.05	2.03	2.02	2.03	2.03	1.99	1.99	2.03	2.05	2.02	2.05	1.99	2.07	2.02	1.99
Cr	0.00	0.00	0.00	0.00	0.00	0.00	0.00	0.00	0.00	0.00	0.00	0.00	0.00	0.00	0.00	0.00	0.00	0.00	0.00	0.00
Fe^{+3}	0.17	0.05	0.11	0.15	0.14	0.16	0.00	0.00	0.06	0.07	0.03	0.02	0.00	0.10	0.00	0.05	0.01	0.02	0.00	0.00
Fe^{+2}	1.73	1.87	1.78	1.82	1.79	1.71	1.83	1.84	1.81	1.85	1.90	1.63	1.67	1.57	1.59	1.60	1.63	1.64	1.64	1.66
Mn	0.43	0.44	0.45	0.42	0.44	0.49	0.44	0.40	0.43	0.41	0.42	0.62	0.61	0.63	0.62	0.61	0.61	0.61	0.64	0.63
Mg	0.50	0.43	0.47	0.46	0.44	0.49	0.48	0.43	0.45	0.48	0.43	0.51	0.48	0.44	0.44	0.51	0.53	0.47	0.48	0.46
Ca	0.22	0.22	0.23	0.22	0.23	0.20	0.21	0.26	0.24	0.22	0.23	0.23	0.22	0.27	0.26	0.22	0.22	0.23	0.20	0.22
Na	0.00	0.00	0.00	0.00	0.01	0.00	0.01	0.00	0.01	0.00	0.00	0.00	0.00	0.00	0.00	0.00	0.00	0.00	0.00	0.00
K	0.00	0.00	0.00	0.00	0.00	0.00	0.00	0.00	0.00	0.00	0.00	0.00	0.00	0.00	0.00	0.00	0.00	0.00	0.00	0.00
Ni	0.00	0.00	0.00	0.00	0.00	0.00	0.00	0.00	0.01	0.00	0.00	0.00	0.00	0.00	0.00	0.00	0.00	0.00	0.00	0.00
Total	8.00	8.00	8.00	8.00	8.00	8.00	8.00	7.97	8.00	8.00	8.00	8.00	8.00	8.00	7.97	8.00	8.00	8.00	7.99	7.98
XMg	0.04	0.05	0.05	0.05	0.05	0.04	0.05	0.05	0.05	0.05	0.05	0.04	0.04	0.05	0.05	0.04	0.04	0.04	0.04	0.05
XCa	0.10	0.10	0.10	0.10	0.10	0.11	0.11	0.09	0.09	0.10	0.10	0.10	0.10	0.09	0.09	0.10	0.10	0.10	0.11	0.10
XFe	0.01	0.01	0.01	0.01	0.01	0.01	0.01	0.01	0.01	0.01	0.01	0.01	0.01	0.01	0.01	0.01	0.01	0.01	0.01	0.01
Fe T	1.90	1.91	1.89	1.96	1.93	1.87	1.83	1.84	1.87	1.91	1.92	1.65	1.67	1.67	1.59	1.64	1.64	1.66	1.64	1.66

Table 4. Whole rock analysis of the Pamuru granite.

Sample Ref. No.	**SiO_2**	**Al_2O_3**	**Fe^2O_3**	**MnO**	**MgO**	**CaO**	**Na_2O**	**K_2O**	**TiO_2**	**P_2O_5**	**Na_2O+K_2O**	**Sum**	**LOI**
PCS-17	70.80	13.91	1.83	0.02	0.50	2.12	6.41	3.10	0.21	0.04	9.51	98.94	1.06
PCS-4	69.32	14.11	2.67	0.02	0.34	1.83	6.45	4.70	0.38	0.04	11.15	99.86	0.14
PCS-5	70.51	13.54	1.62	0.01	0.79	1.82	6.57	4.19	0.37	0.05	10.76	99.47	0.53
PCS-12	68.74	12.96	2.44	0.05	0.27	2.86	3.72	4.95	0.29	0.05	8.67	96.33	3.67
PCS-15	71.52	13.88	2.83	0.04	0.28	1.52	3.92	4.28	0.33	0.05	8.20	98.65	1.35
PCS-16	69.81	15.06	2.23	0.04	0.78	1.65	4.12	5.36	0.53	0.09	9.48	99.67	0.33
PCS-18	66.50	13.22	3.59	0.03	0.91	4.09	5.97	1.27	0.41	0.04	7.24	96.03	3.97
PCS-26	68.76	15.87	3.56	0.07	0.64	1.91	4.38	4.00	0.44	0.07	8.38	99.70	0.30
PCS-27	69.54	14.86	3.18	0.02	0.59	0.53	4.28	5.31	0.39	0.08	9.59	98.78	1.22
PCS-19	70.10	14.00	2.80	0.05	0.50	1.92	6.10	4.10	0.25	0.04	10.20	99.86	0.14
PCS-8	69.78	14.14	3.70	0.02	0.36	1.72	6.00	3.70	0.38	0.04	9.70	99.84	0.16
PCS-6	70.49	13.15	2.62	0.06	0.80	1.82	6.57	2.19	0.39	0.05	8.76	98.14	1.86
PCS-14	69.40	13.00	2.86	0.05	0.25	2.86	3.72	4.95	0.34	0.05	8.67	97.48	2.52
PCS-19	71.50	14.12	2.79	0.04	0.29	1.59	4.96	3.88	0.39	0.05	8.84	99.61	0.39
PCS-22	69.91	15.26	2.43	0.03	0.67	1.57	3.98	5.16	0.48	0.09	9.14	99.58	0.42
PCS-28	66.58	13.24	3.67	0.03	0.96	4.09	5.84	2.74	0.42	0.04	8.58	97.61	2.39
PCS-11	69.12	15.75	3.58	0.06	0.58	1.91	4.29	4.11	0.49	0.07	8.40	99.96	0.04
PCS-2	69.14	14.98	3.22	0.04	0.61	0.53	4.35	4.93	0.42	0.08	9.28	98.30	1.70

e-ISSN: 2583-6900

Table 6. Rare earth analysis of Pamuru granite.

Sample Ref. No.	La	Ce	Pr	Nd	Eu	Sm	Tb	Gd	Dy	Ho	Er	Tm	Yb	Lu	Hf	Ta	W	U	TREE
PCS-17	157.73	140.44	15.24	59.60	1.63	11.22	2.41	12.47	17.08	3.69	12.41	1.93	12.99	2.09	28.12	3.68	7.29	6.72	450.92
PCS-4	240.61	432.11	48.42	182.80	2.03	34.36	5.62	32.98	34.05	6.85	21.69	3.42	21.12	3.19	30.17	4.71	5.00	6.75	1069.24
PCS-5	102.68	213.63	23.73	85.74	1.44	15.42	2.73	15.59	17.20	3.52	11.15	1.70	10.55	1.68	27.28	3.54	5.00	11.80	506.76
PCS-12	105.10	232.23	24.14	95.10	1.83	19.04	3.49	19.98	22.49	4.56	14.07	2.23	14.38	2.21	29.98	3.79	5.00	5.61	560.83
PCS-15	186.93	450.77	41.72	162.75	5.00	33.80	7.07	38.79	47.34	9.87	30.44	4.65	29.51	4.38	30.13	3.13	7.75	11.99	1053.04
PCS-16	127.90	475.48	29.79	110.37	1.83	21.68	4.05	21.96	27.93	5.79	19.54	3.21	22.01	3.15	30.06	4.40	5.00	9.47	874.70
PCS-18	194.08	453.16	42.93	170.19	4.07	31.67	3.83	27.70	18.20	2.81	6.76	0.91	5.66	1.04	27.89	4.14	5.35	6.04	963.02
PCS-26	155.47	342.19	38.95	148.21	3.47	29.29	4.95	27.71	32.11	6.45	19.43	2.90	17.04	2.50	28.54	4.22	14.36	5.55	830.69
PCS-27	189.09	358.22	35.37	133.11	1.88	25.22	4.66	25.78	30.91	6.46	20.03	3.22	20.16	3.16	28.97	4.09	12.61	9.84	857.28
PCS-19	170.73	214.44	35.23	89.37	2.13	15.28	3.40	32.67	24.27	4.17	22.15	0.93	13.65	2.85	27.18	4.64	6.13	9.22	631.28
PCS-8	238.61	342.11	47.19	178.86	2.79	36.34	5.09	31.81	37.70	5.98	26.60	2.18	19.99	3.06	29.70	4.67	5.32	6.98	978.31
PCS-6	112.68	403.63	36.99	89.39	1.98	14.12	4.89	18.94	27.05	3.75	17.88	1.90	11.51	2.65	25.85	3.24	4.96	10.98	747.35
PCS-14	125.10	321.23	25.15	105.98	1.86	20.18	2.94	20.76	29.91	4.16	19.68	3.12	15.04	2.06	30.10	4.12	5.00	6.14	697.15
PCS-19	189.93	449.66	45.22	165.15	4.86	32.39	6.85	36.24	45.34	8.90	20.17	4.45	29.14	4.78	30.11	3.93	7.78	10.95	1043.07
PCS-22	136.90	479.83	41.31	129.76	1.89	29.58	5.14	25.98	24.45	5.23	22.40	3.30	22.60	4.06	30.05	4.35	5.87	10.47	932.44
PCS-28	202.08	455.61	44.93	176.74	4.98	30.27	3.89	29.10	20.17	2.98	16.88	1.91	15.16	1.35	26.18	3.98	5.46	8.37	1006.06
PCS-11	175.47	432.88	39.54	152.29	4.37	30.94	5.16	27.35	30.23	6.02	23.69	2.94	17.47	2.41	29.14	4.29	13.97	7.93	950.74
PCS-2	196.09	389.55	36.10	146.94	1.90	28.20	4.94	29.23	34.20	6.96	22.19	3.26	18.84	4.60	28.69	4.20	12.37	10.13	923.00

Table 5. Trace element analysis of the Pamuru granite.

Sample Ref. No.	Ba	Ga	Sc	V	Th	Pb	Ni	Co	Rb	Sr	Y	Zr	Nb	Cr	Cu	Zn	Be	Ge	Mo	Sn
PCS-17	561	22	4	20	70	10	2	4	102	81	146	992	37	15	1	10	2.44	0.93	0.3	5.00
PCS-4	1329	31	4	20	84	9	16	4	96	91	193	970	59	15	4	14	3.13	1.37	0.30	5.00
PCS-5	455	21	5	38	59	8	13	32	85	67	98	1021	43	15	1	10	1.72	0.72	0.30	5.00
PCS-12	864	25	6	20	38	20	2	7	127	46	116	555	50	15	8	25	1.76	1.26	0.30	5.00
PCS-15	2041	23	5	20	63	30	2	5	126	94	199	823	28	15	5	93	1.98	1.19	0.30	5.00
PCS-16	1043	19	6	20	68	16	9	10	93	44	164	698	75	15	18	14	2.13	0.87	0.30	5.00
PCS-18	751	25	4	20	48	17	2	4	97	176	106	1017	16	15	3	55	1.85	0.82	0.30	5.00
PCS-26	1472	25	6	20	58	22	6	6	83	80	160	735	29	15	27	83	2.96	1.09	0.30	5.00
PCS-27	682	24	4	20	73	18	2	2	132	30	180	834	69	15	1	20	2.11	1.04	0.30	5.00
PCS-19	631	34	6	20	69	12	6	5	89	145	176	1019	39	15	1	10	2.13	0.99	0.3	5.00
PCS-8	1331	36	5	20	92	11	19	7	117	119	197	948	60	15	5	16	2.98	1.34	0.30	5.00
PCS-6	48063	28	5	32	65	9	16	30	105	123	102	1018	46	15	8	13	1.77	0.77	0.30	5.00
PCS-14	864	35	6	20	43	24	13	9	127	98	156	574	52	15	1	30	2.16	0.96	0.30	5.00
PCS-19	2039	33	5	23	65	34	15	8	126	109	199	839	31	15	4	89	2.08	1.27	0.30	5.00
PCS-22	1034	29	4	20	78	26	10	15	93	102	134	704	73	15	16	17	2.21	0.89	0.30	5.00
PCS-28	749	28	5	21	50	20	6	5	125	176	156	1013	19	15	4	45	1.92	0.87	0.30	5.00
PCS-11	1454	23	4	25	53	27	9	8	119	112	168	748	27	15	20	78	1.96	1.19	0.30	5.00
PCS-2	680	22	6	22	75	19	8	9	132	106	189	871	71	15	1	24	2.31	1.24	0.30	5.00

and uranium (U). For EPMA analysis Signal(s) Used: Y La, P Ka, Si Ka, Th Ma, U Mb, Ca Ka, La La, Ce La, Pr La, Nd La, Sm La, Gd La, Pb Ma, Eu La, Tb La, Yb La. Specific beam conditions, such as 20 kV, 50 nA, and 5 µm spot size are used for calibration and analysis. For U-Th-Pb Geochronology, EPMA is used to analyse the U-Th-Pb ratios within monazite, allowing for the calculation of crystallization ages. This is often combined with TIMS-U–Pb isotope analysis for more precise age determinations. Standards for U, Th, and Pb (e.g., PbS, UO_2, ThO_2) are employed for calibration. Measured elements area Pb Ma with overlapping elements are Th Mz and standard used Th glass. Synthetic silica-aluminium glass with REEs is used for REE analysis. Interference corrections are applied for U and Pb analysis on PETL crystals. Monazite age populations are calculated using weighted average routines, with errors typically less than 10 Ma for Paleozoic monazite. Monazite grain for Progress Granite from Larsemann Hills, Antarctica was used as internal proxy standard.

5. Results

5.1. Mineral Chemistry

Pamuru granite (PG) shows two micas, feldspar and garnet as common mineral phases. The mineral composition of different minerals has been assessed through EPMA study and presented in Supplementary Tables No 1 to 3.

Plagioclase feldspars show restricted composition and plotted in the field of andesine within the range of albite to anorthite. Likewise, potash feldspar is restricted to the orthoclase extreme end (Fig. 4a, Table 1). Plagioclase shows a high content of Ca (0.346–0.365), Na (0.592–0.656), Al (1.358–1.375), very low K (0.002–0.005) content in apfu and shows the range of $Ab_{61.67–65.35\%}$ $An_{34.41–37.76\%}$ $Or_{<0.5\%}$ content, respectively (Fig. 4a, Supplementary Table 1). The potash feldspar shows a high content of K (0.006–0.973), Al (0.955–0.999), Na (0.042–1.333), content in apfu and shows the range of $Ab+An_{04.1–09.9\%}Or_{90.1–95.9\%}$ content, respectively (Fig. 4a, Table 1).

Mica in the PG is commonly in association with an interstitial to the feldspar and quartz. Biotite has a restricted but high range of Mg (3.26–3.47), Fe^T (1.35–1.55), high K (0–0.01), moderate Al (3.16–3.21), and Ti (0.50–1.3) content in apfu, respectively. Its composition is straddled in between the ferro-biotite and Magnesio-biotite in the Fig. 4b. Similarly, in the TiO_2*10- (FeO+MnO)–(MgO) triangular diagram all biotite plotted in the primary field (Fig. 4c). In contrast, muscovite has a restricted moderate to low range of Mg (0.17–0.19), Al (5.28–5.45), Fe^T (0.26–0.34), and high K (1.26–1.66) and Ti (0.02 to 0.05) content in apfu (Table 2).

The garnets are euhedral to subhedral in shape and generally iron-manganese rich in nature with almandine composition (Fig. 4d). It has high range of Fe^T (1.59–1.96 in apfu), Mn (0.40–0.64 in apfu), Al (1.99–2.07 in apfu), and CaO (0.21–0.26) with X_{Mg} (0.04–0.05), X_{Ca} (0.09–0.111), X_{Fe} (0.01), content, respectively (Table 3).

5.2. Whole-rock Geochemistry

Geochemistry of PG show high range of SiO_2 from 66.50 wt % to 71.52 wt %, Al_2O_3 from 12.96 wt % to 15.87 wt %, with (Na_2O + K_2O) from 6.51 wt % to 9.59 wt %. It has low CaO from 0.53 wt % to 2.79 wt % except one 4.09, and MgO from 0.27 wt % to 2.79 wt %, (Table 4). In the TAS diagram, they fall typically in the granite field (Fig. 5a), following the high calc-alkaline to shoshonite trend with a strong affinity to the shoshonite fields with > 3 wt % of K_2O content (Fig. 5b). The molar percentage clearly exhibit strongly peralkaline with trend follows peraluminous nature with A/NK and A/CNK ratios > 1% (Fig. 5c). They are typically plotted into the ferroan field and also in the field of TBTZ (1.2 Ga) granite (Fig. 5d).

Trace element analyses of PG reveal enriched Ba (61–2041 ppm), Rb (5–132 ppm), Sr (30–176 ppm), Zr (555–1021 ppm), Pb (4–30 ppm), Y (56–199 ppm) and significant content of La (57.73–240.61 ppm), Ce (140.44–475.48 ppm), Nd (59.60–170.19 ppm) with higher content of total REE content (349.92–1069.24 ppm) (Tables 5 and 6). The multi-elemental, primitive mantle normalized plot of PG shows the strong depletion of Ba, Rb, Nb, Pb, Sr, P, Sr and Ti elements (Fig. 6a). It also has normalized ratios of La/Yb (3.87–8.88), La/Sm (2.84–8.64), Ce/Yb (2.75–8.91), Ce/Sm (2.20–6.70), Eu/Yb (0.23–2.05) and Eu/Eu* (0.18–0.51). The REE chondrite normalized plot shows strong enrichment of LREE with a strong negative Eu anomaly and flat HREE pattern (Fig. 6b).

In R_1 versus R_2 tectonic discrimination diagram, PG show the late-orogenic setting (Fig. 7a, after

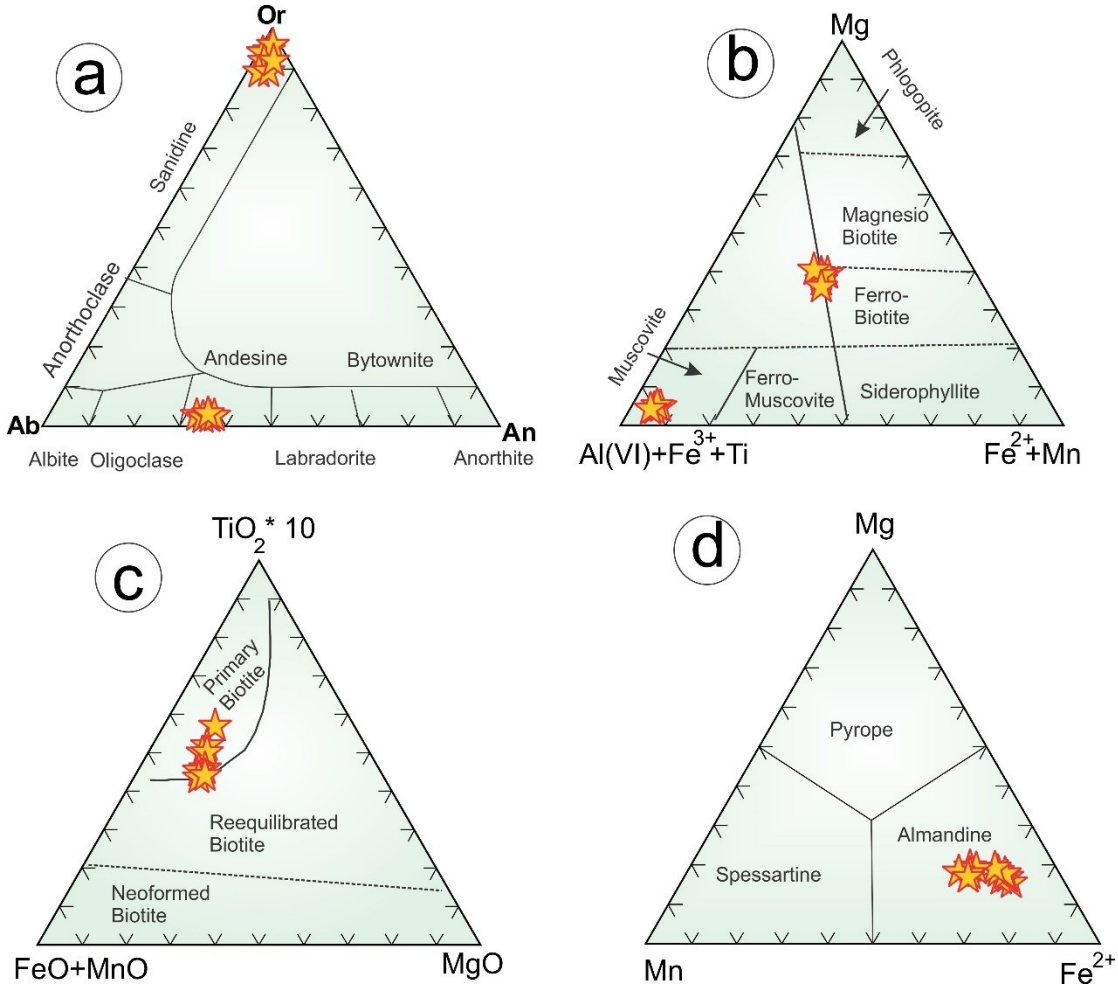

Fig. 4. a) Position of K-feldspar and plagioclase of Pamuru Granite in Ab–An–Or diagram (Smith and Brown, 1988). b) Mg-(Al^{VI}+Fe^{3+}+Ti) -(Fe^{2+}+Mn) diagram (after Foster, 1960), c) 10×TiO^2-(FeO+MnO)-MgO (after Nachit et al., 2005), d) Mg-Mn-Fe^{2+} ternary diagram of garnet.

Batchelor and Bowden, 1985). Their tectonic nature is getting clearer in Y versus Nb plot in which PG clearly plot in the within plate granite (WPG) setting (Fig. 7b). Its within plate nature is also supported by the Hf–Rb/30-Ta*3 diagram in Fig. 7c. The PG shows a strongly differentiated nature as supported by the Ba–Rb–Sr triangular plot (Fig. 7d). Furthermore, PG have high (Na_2O+ K_2O/CaO) ratio and high FeO^t content with typical peraluminous and enriched Ba, Zr, Y, Rb with high REE content and low Sr content indicates reveals anorogenic nature (Whalen et al., 1987) and A-type granitic signature (Fig. 8a–c). It is further classified as A_2 type granite by Y–Nb-3*Ga, and Y–Nb–Ce ternary diagrams (Fig. 8d–e).

5.3. Monazite Mineral Chemistry

We have reported a single grain of monazite and which is rounded in nature and exhibit zoning with a brighter core and dark rim, with the development of cracks (Fig. 9). Carried out 8 points analyses, which are distributed in two compositional domains, i.e, a core part analysis, where show P_2O_5 is the most abundant oxide ranging from 29.40–30.76 wt%. Other ranges include Y_2O_3 from 1.49 to 2.63 wt%, ThO_2 from 6.62 to 13.82 wt%, UO_2 from 0.33 to 0.68 wt%, La_2O_3 from 10.10 to 12.55 wt%, Ce_2O_3 from 22.32 to 26.09 wt%, with restricted range of Pr_2O_3 from 10.03 to 10.32 wt%, SmO from 2.18 to 2.41 wt%, Gd_2O_3 from 2.18 to 2.41 wt%, PbO from 0.62 to 1.11 wt%, Tb_2O_3 from 0.11 to 0.16 wt%, and Yb_2O_3 upto 0.021 wt%. Monazite have (REE^{3+}, Th^{4+}, U^{4+}, Ca^{2+}, Pb^{2+}) PO_4 formula show Primary coupled substitution ie., Th + Ca^2 2 REE^3 as balance charge as supported significant ThO_2 and CaO concentration without SiO_2. SiO_2 is 0, indicate no charge compensation via Si on the P-site. The significant presence of ThO_2 (6.62–13.82 wt%) and UO_2

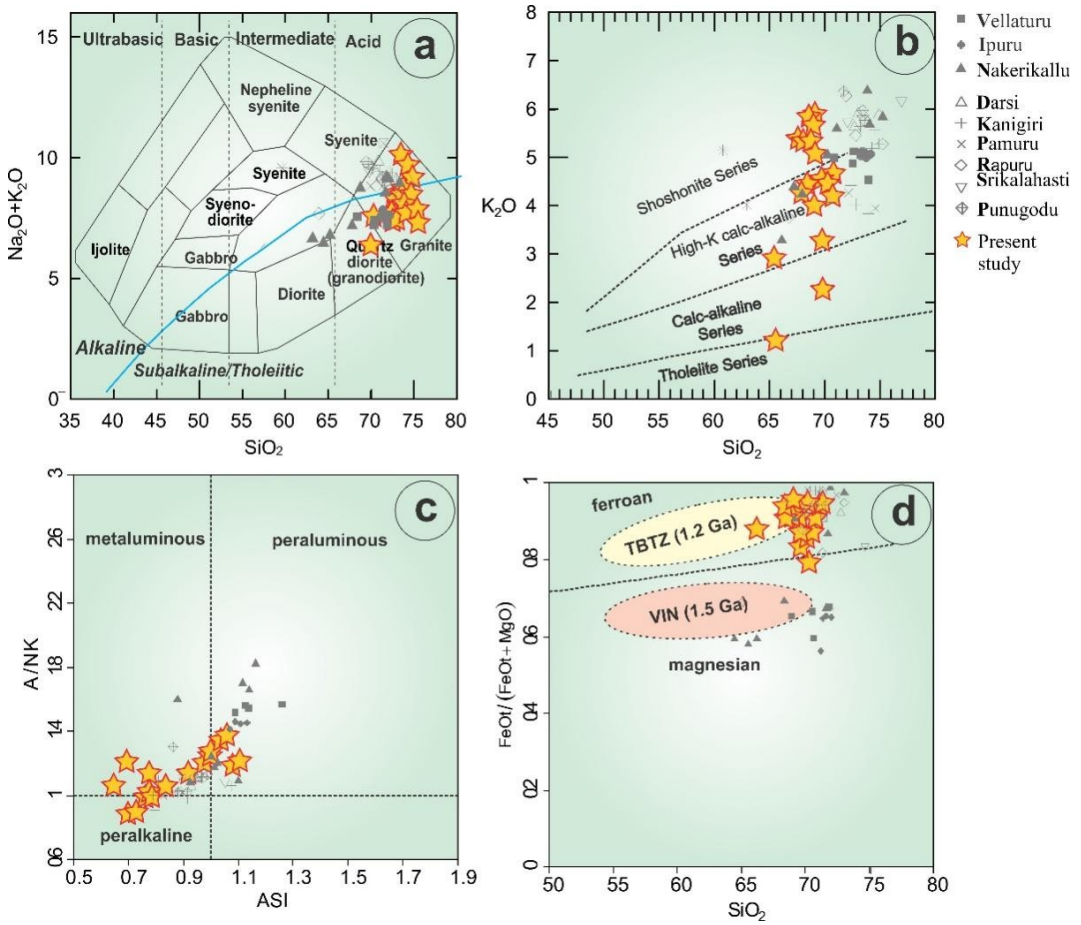

Fig. 5. a) Position of the Pamuru granites in TAS diagram. b) Plot showing the High-K calc-alkaline to shoshonite character of the Pamuru granites correspond to biotite compositions. c) Granites are straddled in the metaluminous to peraluminous field correspond to biotite compositions (Maniar and Piccoli, 1989). d) Plot showing ferroan affinity to the Pamuru granite (field of TBTZ and VIN granite, Sesha Sai, 2023).

(0.33–0.68 wt%) indicates substantial substitution of REE^{3} by tetravalent actinides. PbO values (0.62–1.11 wt%) suggest partial substitution of REE^{3} by radiogenic Pb^{2}. REE = Rare Earth Elements like primarily Ce, La, Nd, Pr, and sometimes Sm, Gd, Y, etc., exhibit a monoclinic structure; hence, the trivalent rare earth element (REE^{3+}) cation occupies the A-site in the crystal lattice.

In contrast, rim part analysis shows P_2O_5 is the most abundant oxide ranging from 28.65–30.17 wt%. Other ranges include ThO_2 from 7.25 to 8.58 wt%, UO_2 from 0.13 to 0.14 wt%, La_2O_3 from 15.02 to 16.22 wt%, Ce_2O_3 from 27.13 to 27.23 wt%, with restricted range of Pr_2O_3 from 03.40 to 03.31 wt%, Y_2O_3 from 0.33 to 0.35 wt%, SmO from 1.22 to 1.40 wt%, Gd_2O_3 from 2.92 to 2.98 wt%, PbO from 0.16 to 0.19 wt%, Tb_2O_3 upto 0.04 wt%, and Yb_2O_3 upto 0.01 wt%.

6. Discussion

6.1. Chemical (Th–U–Pb) monazite age

Geochronological data from various locations in the Cuddapah Basin and adjacent regions indicate a complex thermal and magmatic history spanning from the Paleoproterozoic to the Mesoproterozoic. At Vinukonda, U–Pb dating yields an age of 1589.7 ± 5.7 Ma, while Rb–Sr isotopic analysis provides a slightly older age of 1615 ± 25 Ma (Dobmeier et al., 2006; Gupta et al., 1984). The Dekanakonda-Torakonda region also records a similar Rb–Sr age of 1615 ± 25 Ma (Gupta et al., 1984), suggesting a regionally significant magmatic-thermal event. Moreover, Dobmeier et al. (2006) reported ages from Vinukonda granite exhibit upper intercepts at 1588.4 ± 7.1 and 1589.7 ± 5.7 Ma, interpreted to date magma emplacement. In contrast, reported ages at 501–474 Ma are indicative of low-grade metamorphic overprint.

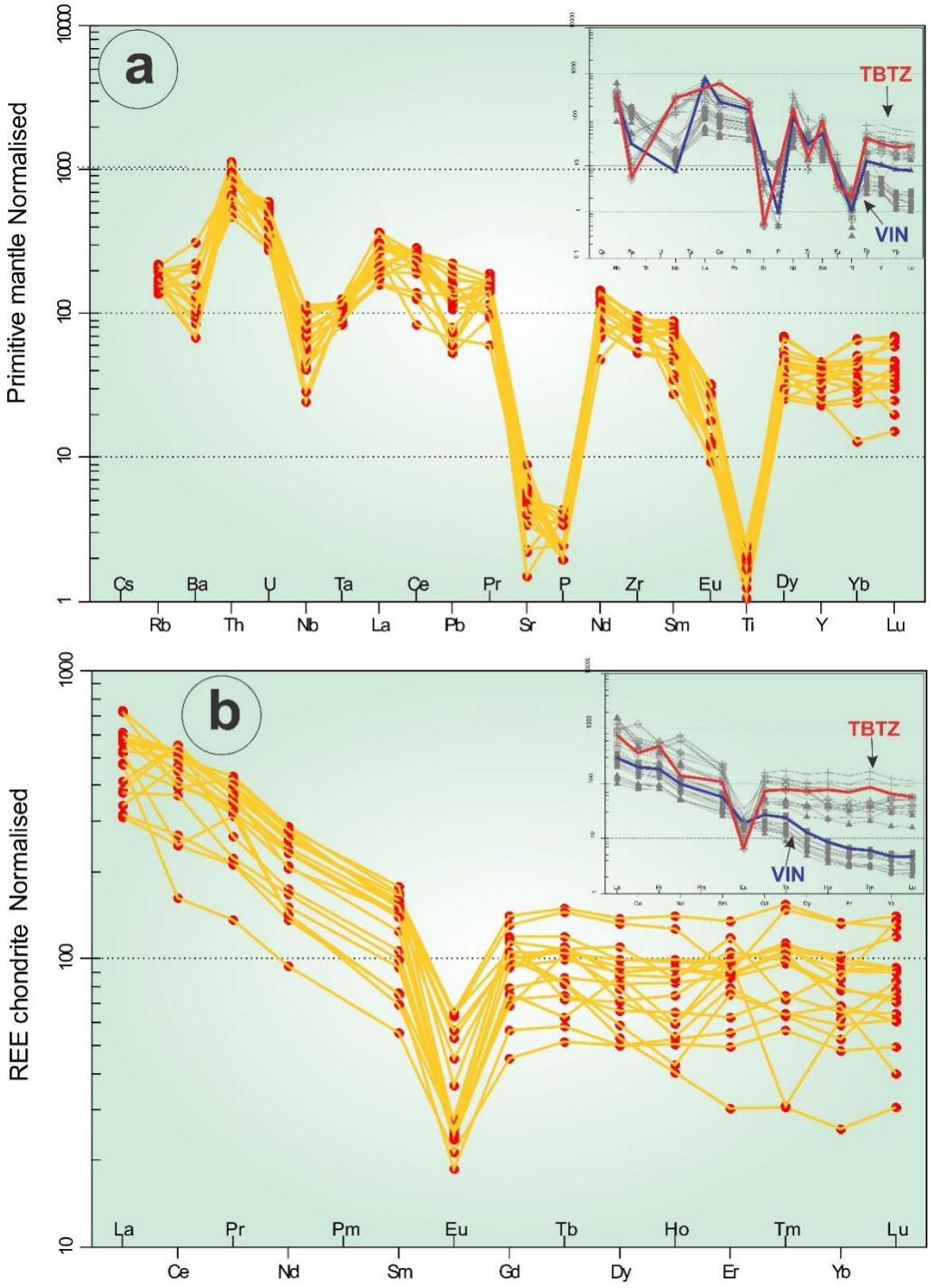

Fig. 6. a) Primitive Mantle normalized plot for Pamuru granite (Sun and McDonough, 1989). b) Chondrite-normalized plot for Pamuru granite (Nakamura, 1974).

Further south, the Kanigiri area exhibits younger Rb–Sr ages of 1120 ± 25 Ma and 1330 Ma, the latter based on recent geochronological refinement (Gupta et al., 1984; Dharma Rao and Santosh, 2011). Likewise, Sain et al. (2017) provided similar ages around 1284 Ma for the Kanigiri granite. Recently, Narshimha et al. (2022) reported the ages from zircon U–Pb at 1257 ± 6 Ma from Punugodu granite, suggesting magmatic emplacement ages. Further, Narshimha and Kumar (2024) refer to the emplacement of Kanigiri granitic magma along the syntectonic deep crustal shear within Nellore Schist Belt,

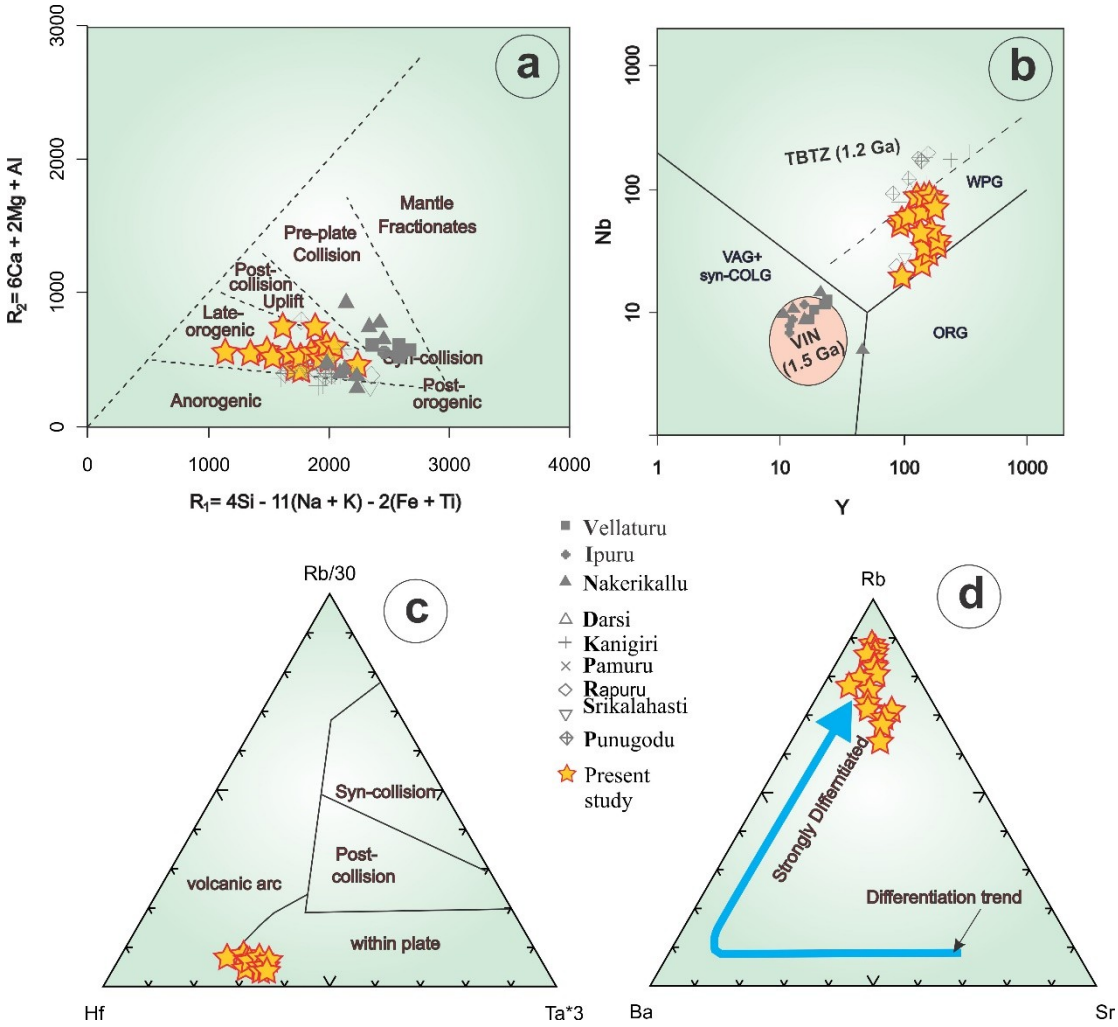

Fig. 7. a) Geochemical R1–R2 plot showing the late-collisional nature of Pamuru granites (Batchelor and Bowden, 1985). b) Y–Nb plots showing the Within Plate Granite (WPG) nature of the Pamuru granite (Pearce et al., 1984). c) Ternary Hf–Rb/30-Ta*3 diagram exhibit the data in the Within Plate and volcanic arc (Harris et al., 1986). d) Ba–Rb–Sr ternary diagram represents the strongly differentiated trend of Pamuru granite (after, El Bouseily and El Sokkary, 1975).

Southern India. These data collectively reflect multiple episodes of magmatism and metamorphism that have influenced the tectono-thermal evolution of the region.

The monazite grain in the PG shows a rounded nature with corroded grain boundaries. The development of the zone as a dark outer rim compared to the bright core is clearly observed in the monazite (Fig. 9). Eight analyses were carried out on a single grain to delineate the age difference between the core and rim of monazite. However, two uniform age domains were obtained from this monazite grain rim and core portions. Both the portions have distinct composition of ThO_2, UO_2, La_2O_3, Ce_2O_3, Pr_2O_3, Y_2O_3, SmO, Gd_2O_3, PbO concentrations resulting into the age variations (Table 7). The Th/U ratios also play a vital role in understanding the behaviour or nature of monazite grains ie., Magmatic monazite typically shows high Th/U ratios, often in the range >20, sometimes as high as 30–100. Such higher ranges are reported in the monazite of Pamuru granite, which ranges from 10.40 to 42.20 (Table 7). Such variations in single grains (core to rim) also show variation in the PbO/ThO_2 ratios corroborated with the reported range ages i.e., 1567–1681 Ma and 511–513 Ma. The 1567–1681 Ma from PG granite clearly indicating the age of magmatic crystallization, whereas, the 511-513 Ma ages are akin to post magmatic thermal events. The geochemical traits of Pamuru granite akin to the geochemical behaviour of ∼1.2 Ga, TBTZ granite (Fig. 5, Fig. 6). Moreover, Fig. 6 clearly depicts the chondrite normalized pattern similar to the TBTZ granite, ie., enriched LREE with negative europium anomaly and

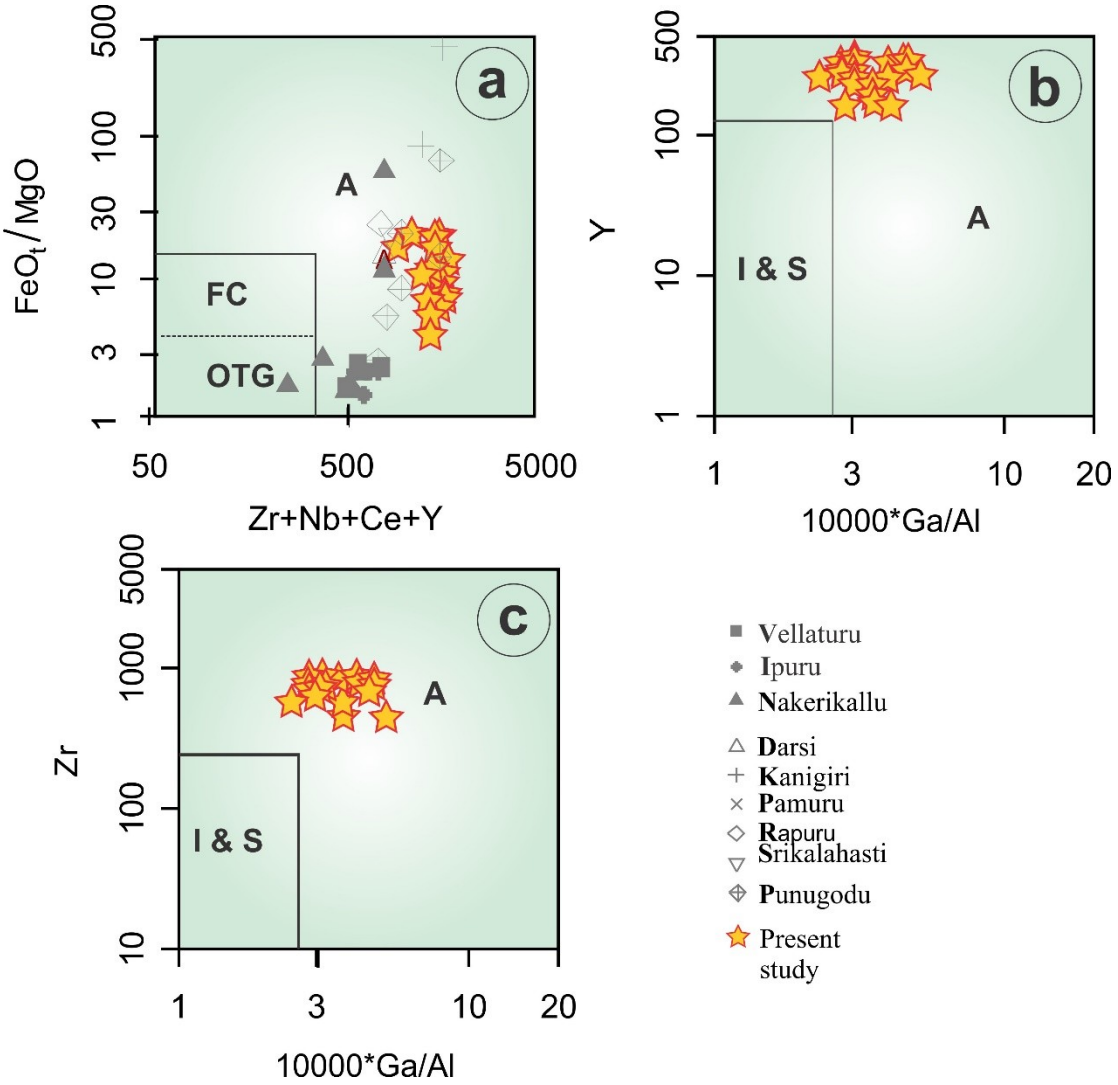

Fig. 8. a) Binary plots of FeO_t/MgO against Zr+Nb+Ce+Y, b) Y against 10000*Ga/Al, c) Zr against 10000*Ga/Al for Pamuru granite shows A-type characters.

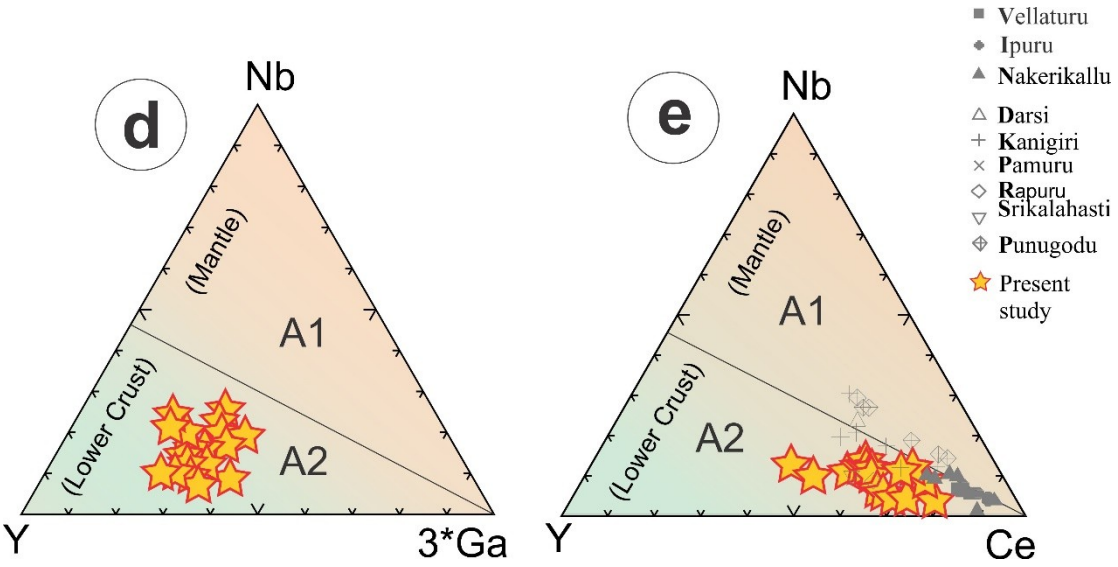

Fig. 8. d) Y–Nb-3*Ga and e) Y–Nb–Ce ternary diagram shows A_2 type classification of Pamuru granites.

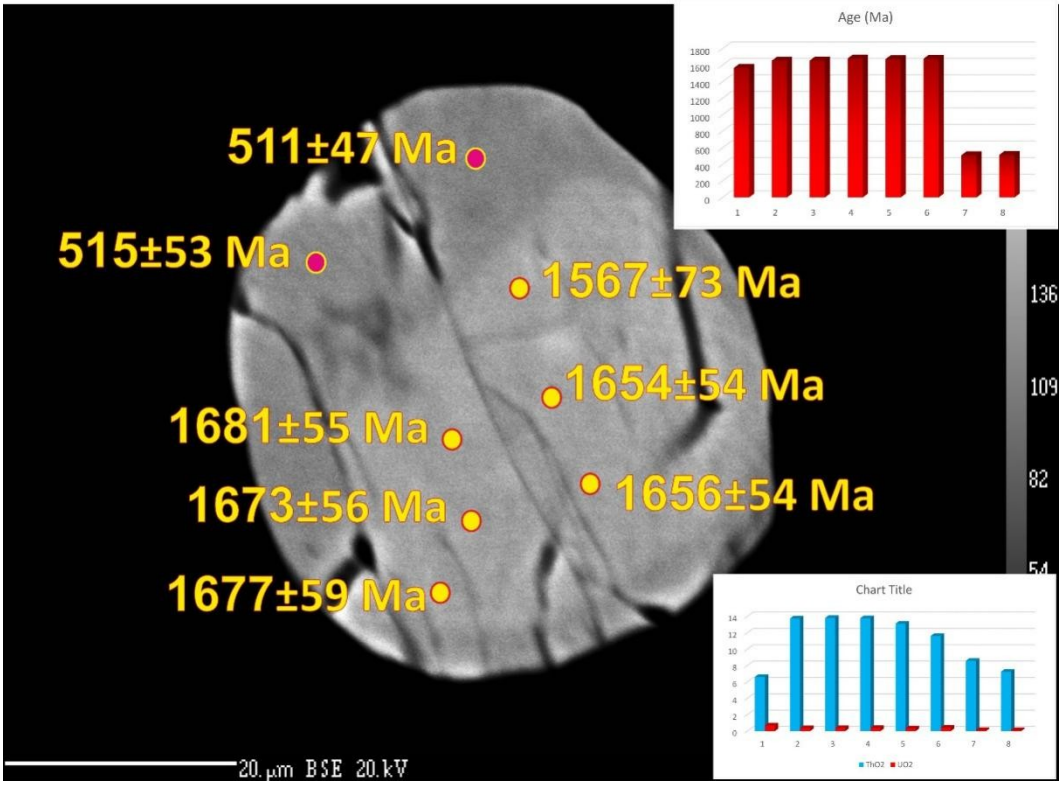

Fig. 9. The back-scattered electron (BSE) image of monazite grain shows the resence of U–Pb–Th chemical ages for the Pamuru granites (Note- histogram shows the representation of ages (in red) and concentration of ThO_2 and UO_2 (in blue)).

flat HREE. However, the above reported ages from the present study ie., 1567–1681 Ma exhibit similarity with VIN granites These variations indicate that the core zone with high thorium concentration reveals the magmatic crystallization ages as substantiated by the ages reported from VIN granite (∼1.5 Ga). Whereas, the rim zone with comparatively low thorium concentration supports the post-magmatic imprints and ages are akin to the Pan-African orogeny. It is also clear from the reported ages that, the PG shows geochemical characteristics like ∼1.2 Ga, TBTZ granite, however, the reported ages from monazite showing affinity to ∼1.5 Ga, VIN granite suggest the xenocrystic nature of monazite. It further reveals that the source for PG granite may be contributed by the lower crustal rock for VIN granite.

6.2. Tectonic setting

Several studies differentiated the Proterozoic Felsic Magmatism in the NFB and adjoining Nellore Schist Belt, Eastern Dharwar Craton based on geochemical characteristic and distinct tectonic settings (Sesha Sai, 2013, 2023). A number of isolated granite plutons that are disposed in a curvilinear emplacement along the western margin of the NSB and are termed as Terrain Boundary Tectonic Zone (TBTZ) granites. Whereas, chain of granite emplacement further north is termed as VIN granites. These Mesoproterozoic felsic intrusive together over a stretch of 350 km from Vinukonda in north to south of Rapur and are disposed along a curvilinear zone along the western margin of NSB. Geochemically, the VIN granites exhibit magnesian feldspathic character and shows emplacement in an arc magmatic tectonic setting. In contrast, TBTZ granites are exhibit ferroan feldspathic character and shows emplacement in a back arc or rift related magmatic tectonic setting. The PG is the part of TBTZ granite system share similar geochemical signature and geodynamic setting, which is discuss further in detail.

A-type granitic nature of PG is clearly depicted from various trace element ratios as discussed in previous section. The A-type granites are exclusively derived from magmas have an igneous source (Whalen et al., 1987) form during the partial melting of granodiorite or tonalite with an extreme fractionation of mafic magmas (Loiselle and Wones, 1979). The several processes are involved during the petrogenesis of the A-type granites, which play a significant role during their evolution in the different terranes. These

Table 7. Representative EPMA (Th–U–Pb) analysis of the monazite grain.

Point	Y_2O_3	P_2O_5	SiO_2	ThO_2	UO_2	CaO	La_2O_3	Ce_2O_3	Pr_2O_3	Nd_2O_3	SmO	Gd_2O_3	PbO	EuO	Tb_2O_3	Yb_2O_3	Total	Age (Ma)	Age err
1 / 1 .	2.64	30.76	0.00	6.62	0.69	1.68	12.56	26.10	3.31	10.28	2.19	3.53	0.62	0.00	0.15	0.02	101.14	**1567**	73
2 / 1 .	1.58	29.61	0.00	13.75	0.37	2.65	10.12	22.51	2.97	10.21	2.28	3.39	1.09	0.00	0.17	0.02	100.72	**1654**	54
3 / 1 .	1.58	29.84	0.00	13.83	0.37	2.60	10.15	22.80	2.92	10.22	2.20	3.26	1.10	0.00	0.11	0.00	100.97	**1656**	54
4 / 1 .	1.65	29.48	0.00	13.80	0.38	2.72	10.10	22.33	2.94	10.04	2.24	3.38	1.12	0.00	0.14	0.00	100.31	**1681**	55
5 / 1 .	1.50	29.92	0.00	13.12	0.34	2.59	10.44	22.93	2.96	10.33	2.13	3.39	1.05	0.00	0.12	0.00	100.81	**1673**	56
6 / 1 .	1.52	29.41	0.00	11.62	0.43	2.36	10.68	23.44	3.06	10.33	2.42	3.66	0.97	0.00	0.16	0.00	100.04	**1677**	59
Point	**Y_2O_3**	**P_2O_5**	**SiO_2**	**ThO_2**	**UO_2**	**CaO**	**La_2O_3**	**Ce_2O_3**	**Pr_2O_3**	**Nd_2O_3**	**SmO**	**Gd_2O_3**	**PbO**	**EuO**	**Tb_2O_3**	**Yb_2O_3**	**Total**	**Age (Ma)**	Age err
1 / 1 .	0.34	28.65	1.45	8.59	0.15	0.78	15.03	27.23	3.41	9.27	1.41	2.98	0.20	0.00	0.04	0.02	99.52	**511**	47
2 / 1 .	0.35	30.18	0.43	7.25	0.13	1.41	16.23	27.13	3.32	8.90	1.22	2.92	0.17	0.00	0.01	0.01	99.67	**515**	53

are combinations of processes like (a) crystal liquid fractionation, (b) incomplete separation of melts and source materials, (c) reaction between melts and surrounding wall rocks, and (d) mixing or mingling of coexisting magmas. Especially, crystal liquid fractionation is crucial in anorogenic (A-type) granite magmas (Clemens et al., 1986; Tatsumi et al., 1986; Whalen et al., 1987; Eby, 1990, 1992; Dostal et al., 2004; Dostal and Chaterjee, 2000). Based on difference in petrogenetic pathways it shows further division of A-type granitoids into A_1 and A_2-types based on Y/Nb ratios. The group with lower Y/Nb ratios (<1.2) known as A_1-type, generally includes felsic rocks, that form in oceanic islands and continental rifts; these granitoids were suggested to form an oceanic island basalt source in an intraplate or rift setting. Nevertheless, the A_2-type designated to the higher Y/Nb ratio (>1.2), such rocks are form by different mechanisms like from an island arc or continental margin basalt source, or from crustal sources such as tonalite or granodiorite, or even by partial melting of crust from which a melt was previously extracted (Eby, 1992).

In Precambrian continental terranes, most of A-type igneous rocks are referred to as anorogenic or cratonic (Lameyre et al., 1974) and are emplaced into anorogenic settings both within plate and along plate margins. These granites presumably represent the most voluminous intraplate silicic magmatism and are often aligned in a linear or semi-linear manner across Precambrian cratons and are known to occur in all continents (e. g. Anderson, 1983; Anderson and Morrison, 1992; Ramo and Haapala, 1995; Rajesh, 2000). The Paleoproterozoic to Mesoproterozoic period has witnessed extensive anorogenic granite magmatism worldwide that resulted in events of significant crustal growth (e.g. Haapala and Rämö, 1999). Such anorogenic magmatism also witnesses along the interface of Cuddapah basin/ Nallamallai Fold belt and NSB in linear fashion and characterized as 1.8 Ga to 1.5 Ga subduction-related arc and ∼1.2 Ga back-arc rift-related felsic magmatism's along TBTZ (Sesha Sai, 2023). Especially, ∼1.2 Ga back-arc rift and extensional mechanism and associated magmatism responsible for intrusive younger granites and alkaline rocks of Prakasham Province along these interface of regional tectonic contact. Such tectonically distinct zones (eg. TBTZ) play avital role for genesis of different magmatism. The PG show shoshonitic, strongly ferroan nature with enriched Ba, Zr, Y and high REE,

relatively low Sr, are characteristics of A-type granites (Whalen et al., 1987; Eby, 1990, 1992). REE geochemistry indicates relative enrichment of LREE and strong negative Eu anomaly. Further, in the Y vs Nb trace element tectonic discrimination diagrams (Pearce et al., 1984) the granite exhibits within plate granite (WPG) characters (Fig. 7b) and in Zr +Nb+Ce+Y vs major oxide and 10000 Al*Ga/Al vs trace element plots samples of the PG fall in A-type field (Fig. 8). In Y–Nb-3*Ga diagram (Fig. 8d) and Y–Nb–Ce diagram (Fig. 8e) the PG plot in A_2-type field (Eby, 1992). As suggested by Eby (1992) this A_2-type may be derived by differentiation of a continental tholeiite, with variable degrees of crustal interaction, or by direct melting of a crustal source indicating the intra-continental and continental margin settings of emplacement as represented by spatial distribution. Similarly, the presence of conspicuous Ta–Nb–Th and Ti negative anomalies in multi-elemental primitive normalised plot clearly suggest the role of subduction related magmatic source for genesis of the PG emplaced in late orogenic to anorogenic tectonic setting. Such subduction-related arc signatures (Nb and Ti negative anomalies) are generally inherited from the VIN granites, which are the result of subduction-related arc magmatism emplaced during ~1.5 Ga along the same regional tectonic zone. The presence of crustal xenoliths of VIN granites also indicates the role of crust-mantle interaction or partial melting of crust from which a melt was previously extracted responsible for such signature in PG.

6.3. Implication for Columbia Break up and Pan African Assembly

The eastern margin of the Indian craton records a complex and multi-stage tectono-magmatic history associated with the assembly and breakup of several supercontinents. Tectonic subdivisions east of the Cuddapah Basin reveal four key episodes: (i) Archean to Paleoproterozoic (2.6–1.8 Ga) granitoids and ophiolitic rocks in the NSB, (ii) Mesoproterozoic (1.6–1.05 Ga) magmatic events such as the Vinukonda Granite and syenitoids in the Prakasam Igneous Province, (iii) Grenvillian-age (1.1–1.0 Ga) orogenic rocks, and (iv) Neoproterozoic to Early Paleozoic (800–500 Ma) magmatism and metamorphism related to Rodinia rifting and Gondwana assembly (Leelanandam, 1990; Reddy et al., 1994; Dobmeier and Raith, 2003; Upadhyay et al., 2006).

Zhao et al. (2002, 2004, 2011) link the 2.1–1.8 Ga orogenic belts globally, including India, to the Columbia supercontinent assembly (Fig. 10a). Supporting this, Paleoproterozoic ages (~2.3–1.8 Ga) are documented from supra-subduction settings along the Western Dharwar Craton (Rekha and Bhattacharya, 2014), and lamprophyres (~2.3 Ga) and alkaline rocks (1.85–1.35 Ga) in the NSB (Meshram et al., 2022; Vijaya Kumar et al., 2011). The 1589 ± 4.4 Ma age of the Vinukonda meta-granite (Dobmeier et al., 2006) aligns with the ~1.65 Ga monazite age of Pamuru Granite (PG) reported in this study (Fig. 10a), suggesting subduction-related crustal accretion between 1.8–1.3 Ga and its link to Columbia's breakup and Rodinia's reconstruction (Fig. 10 b, c) (Powell and Pisarevsky, 2002).

A NE-SW trending rift (~1.5–1.3 Ga) along the craton margin, with possible expression as the Godavari-Pranhita aulacogen, reflects Mesoproterozoic rifting associated with Columbia's breakup (Windley, 1995; Upadhyay, 2007). The PG monazite also records a younger age population (513 ± 50 Ma), consistent with the Pan-African event (~500 Ma), marked by nappe stacking and metamorphism in the NFB (Dobmeier et al., 2006; Sheppard et al., 2017). This Pan-African overprint, also evident in Vinukonda meta-granite (lower intercept ~501 ± 65 Ma), reflects India's integration into Gondwana (Fig. 10d, 11).

Thus, the geochemical and geochronological data from PG and surrounding terranes collectively demonstrate prolonged crustal evolution, marked by magmatic accretion during Columbia's growth (1.8–1.3 Ga), rifting related to Rodinia (~1.5–1.2 Ga), and deformation during Gondwana assembly (~0.5 Ga), confirming the eastern Indian margin's role in global supercontinent dynamics (Figs. 10 and 11).

7. Conclusions

The emplacement of Proterozoic felsic magmatic suites along the cratonic fringe of the Eastern Dharwar Craton, particularly the Pamuru Granite (PG) within the TBTZ domain, offers significant insights into the tectono-magmatic evolution of southern India. Geochemical characteristics of PG-including its high silica content, calc-alkaline to shoshonitic affinity, and ferroan nature-suggest its formation in a post-collisional to late orogenic, within-plate geodynamic setting. The presence of A_2-type anorogenic

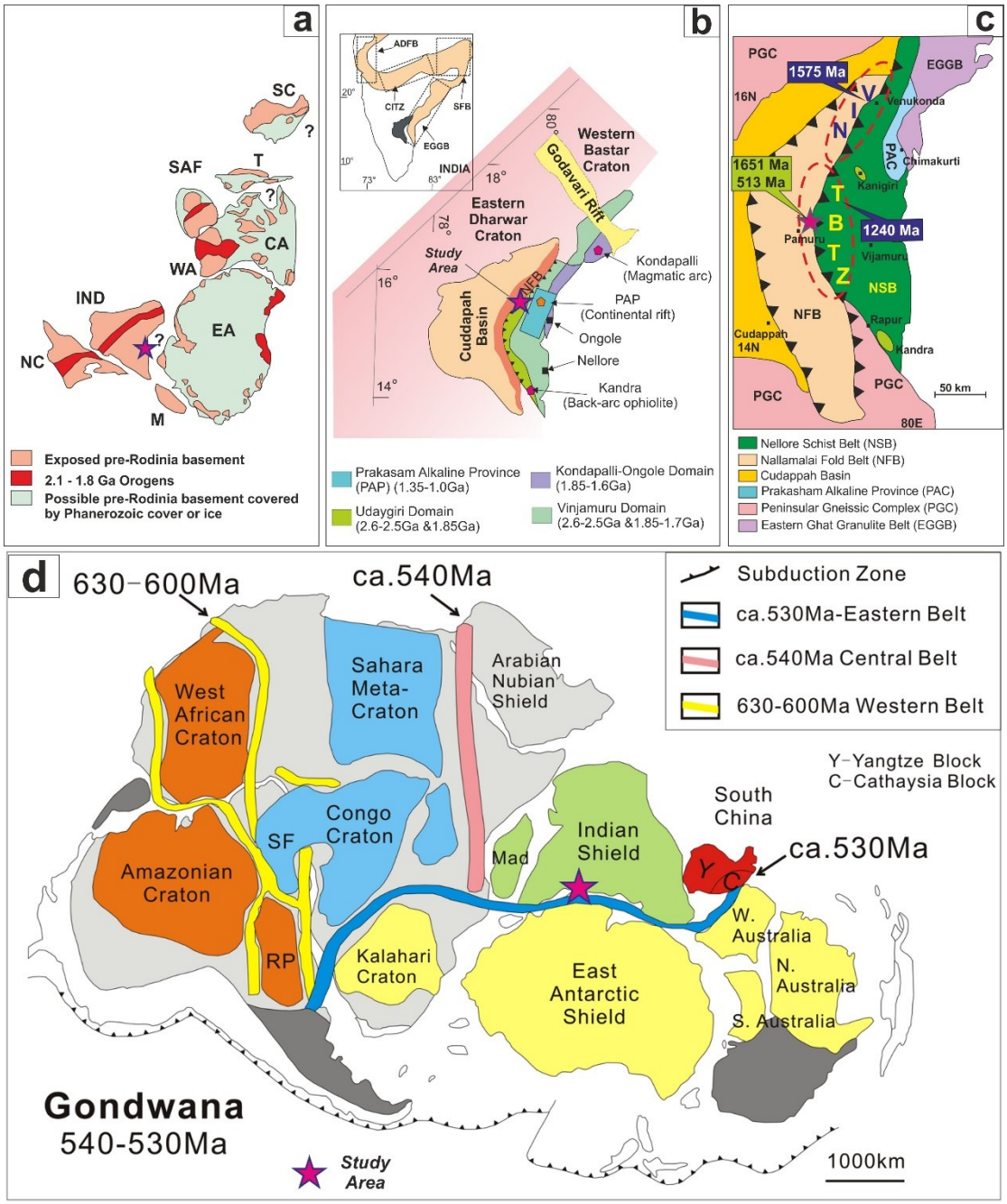

Fig. 10. A possible reconstruction of Paleo-Mesoproterozoic supercontinent Columbia with 1.8–1.3 Ga accretionary orogens (after Zhao et al., 2002) (NC-North China, IND-India, M-Madagascar, EA-East Antarctica, CA-Australia, SAF-South Africa, SC-South China, T-Tarim. a) pre-Rodinia basement b) Generalized geological map of the EGGB with four distinct crustal provinces (modified after Dobmeier and Raith, 2003). Note that the Mesoproterozoic rift magmatism is present between the Vinjamuru and Ongole domains of the Krishna Province (Vijaya Kumar et al., 2011) (Inset map of 1b shows a diagrammatic representation of the Great Indian Proterozoic Fold Belt (GIPFOB; modified after Radhakrishna and Naqvi, 1986) with four distinct mobile/fold belt components. EGGB, Eastern Ghats Granulite Belt; SFB, Singbhum Fold Belt; CITZ, Central Indian Tectonic Zone; ADFB, Aravalli-Delhi Fold Belt. c) Geological Map showing the Regional thrust front along the Cuddapah Basin and NFB as well as in between NFB and NSB Southern India marked by distinct tectonic felsic Proterozoic felsic magmatic zone (VIN and TBTZ). d) Gondwana reconstruction diagram showing the location of Pamuru granite in association with 530 Ma belts (after Santosh et al., 2014).

signatures, along with evidence of highly differentiated magma derived from lower crustal material, points to a rift or back-arc tectonic environment. The monazite grains, with distinct age populations of avg. 1651 ± 58 Ma and avg. 513 ± 50 Ma, links PG to earlier VIN granite emplacement and reflects

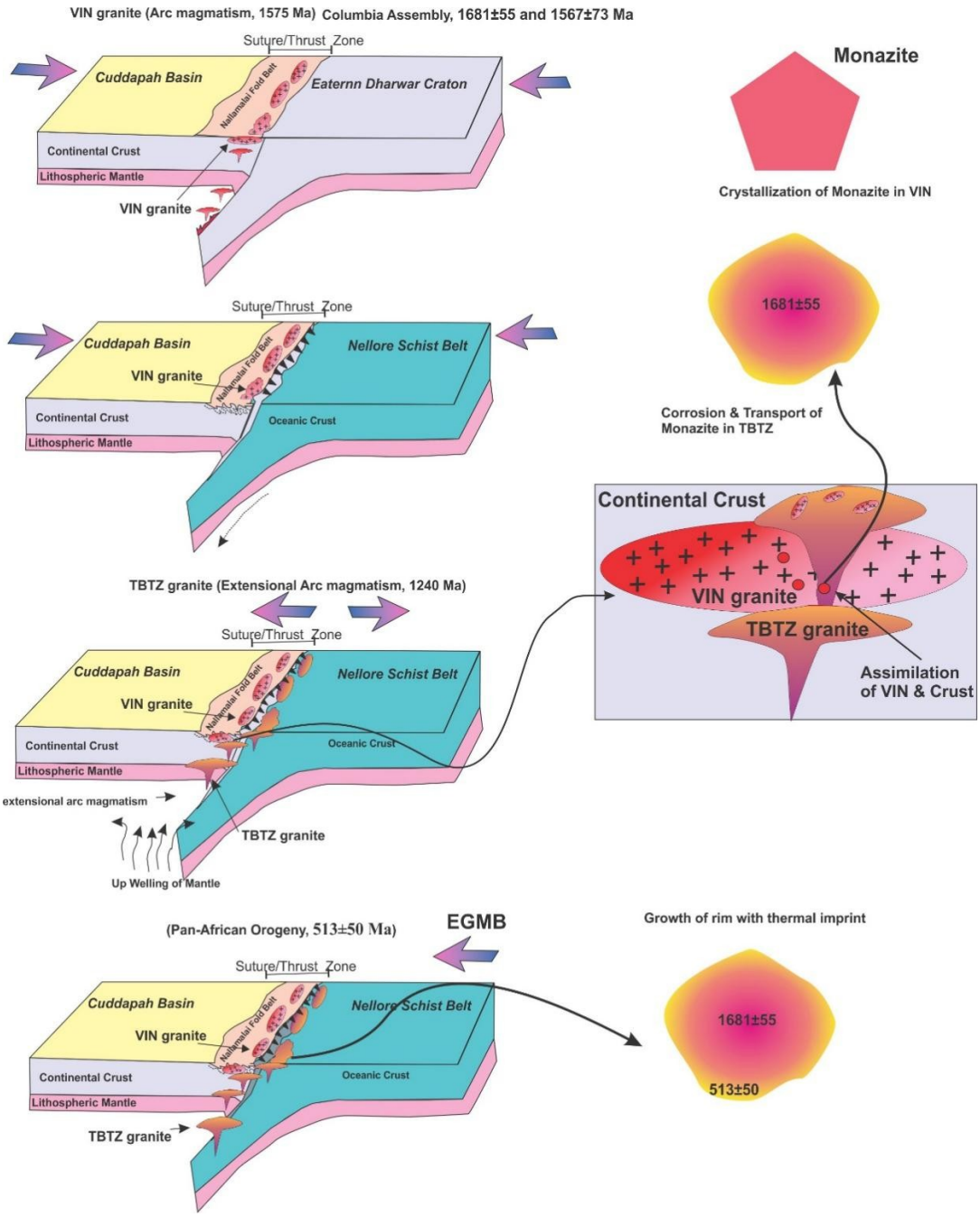

Fig. 11. The schematic diagram exhibits geodynamic processes during Proterozoic felsic magmatism along the interface of NFB and NSB and its relation to the supercontinent Columbia and Pan-African assembly.

both magmatic and metamorphic events. These findings support the existence of a widespread 1.6–1.2 Ga magmatic accretionary belt along the eastern margin of India, relevant to Rodinia supercontinent assembly. Additionally, the recorded Pan-African thermal event around 511–515 Ma signifies the region's geodynamic reactivation during the incorporation of India into the Gondwana supercontinent, highlighting the complex crustal evolution across Proterozoic to Early Paleozoic timescales.

Acknowledgments

The Additional Director General, Geological Survey of India, Southern Region is profusely thanked for allowing work and supporting, and encouragement to publish this work. The authors extend their gratitude to Deputy Director General SU: Andhra Pradesh, & Regional Mission Head-I, SR for providing an opportunity to work in the research area. Authors are thankful to the editor for the consideration of

manuscript for publication in the *J. Geointerface*. We also express our sincere gratitude to Dr. Narshimha Chinthapally, ANRF-National PDF, Department of Geology, Centre of Advanced Study Kumaun University, India for his constructive comments, which helped improve the manuscript.

Data availability statement

The authors confirm that the data supporting the findings of this study are available within the article.

CRediT statement

MVK: project administration (lead), conceptualization (lead), writing – original draft (lead); **TM:** conceptualization (lead), writing -- original draft (lead); **MVK, TK, MM:** project administration, data curation (supporting), investigation (supporting).

Funding/Declaration

This research received no specific grant from any funding agency in the public, commercial, or not-for-profit sectors.

Competing Interests/Ethical statements

The authors declare that they have no known competing financial interests or personal relationships that could have appeared to influence the work reported in this paper.

References

Anderson, J.L., 1983. Proterozoic anorogenic granite plutonism of North America. *Geological Society of America Memoir* 161, 133–154.

Anderson, J.L., Morrison, J., 1992. The role of anorogenic granites in the Proterozoic Crustal development of North America. *Developments in Precambrian Geology* 10, 263–299.

Batchelor, R.A., Bowden, P., 1985. Geochemical R1-R2 plot showing syn-collisional to post-orogenic nature of granites. *Earth and Planetary Science Letters* 74(2-3), 289–301.

Chadwick, B., Vasudev, V.N., Hedge, G.V., 2000. The Dharwar craton, southern India, interpreted as the result of late Archaean oblique convergence. *Precambrian Res* 99, 91–101. https://doi.org/10.1016/S0301-9268(99)00055-8.

Chardon, D., Jayananda, M., 2008. A 3D field perspective on deformation, flow and growth of the lower continental crust. *Tectonics* 27. https://doi.org/10.1029/2007TC002120.(TC1014).

Chetty, T.R.K., 2011. Tectonics of Proterozoic Cuddapah Basin, southern India: A conceptual model. *Jour. Geol. Soc. Ind* 78(5), 446–456.

Chetty, T.R.K., 2017. *Proterozoic Orogens in India: A Critical Window to Gondwana*. Elsevier.

Chetty, T.R.K., Murthy, D.S.N., 1994. Collision tectonics in the late Precambrian Eastern Ghats Mobile Belt: mesoscopic to satellite-scale structural observations. *Terra Nova* 6, 72–81. https://doi.org/10.1111/j.1365-3121.1994.tb00635.x.

Clemens, J.D., Holloway, J.R., White, A.J.R., 1986. Origin of A-type granite: experimental constraints. *American Mineralogist* 7, 317–324. https://doi.org/10.2138/am-1986-4-517.

Dharma Rao, C.V., Santosh, M., 2011. Continental arc magmatism in a Mesoproterozoic convergent margin: petrological and geochemical constraints from the magmatic suite of Kondapalle along the eastern margin of the Indian plate. *Tectonophysics* 510, 151–171. https://doi.org/10.1016/j.tecto.2011.05.019.

Dobmeier, C., Lutke, S., Hammerschmidt, H., Mezger, K., 2006. Emplacement and deformation of the Vinukonda granite - implications for the geological evolution of peninsular India and for Rodinia reconstructions. *Precambrian Research* 146, 165–178. https://doi.org/10.1016/j.precamres.2006.01.011.

Dobmeier, C.J., Raith, M.M., 2003. Crustal architecture and evolution of the Eastern Ghats belt and adjacentregions of India. *Proterozoic East Gondwana: Supercontinent Assembly and Breakup* 206, 145–68. https://doi.org/10.1144/GSL.SP.2003.206.01.09.

Dostal, J., Chaterjee, A.K., 2000. Contrasting behaviour of Nb/Ta and Zr/Hf ratios in a peraluminous granitic pluton Nova Scotia, Canada. *Chemical Geology* 123, 67–88.

Dostal, J., Chaterjee, A.K., Kontak, D.J., 2004. Chemical and isotopic (Pb, Sr) zonation in a peraluminous granite pluton:role of fluid fractionation. *Contributions to Mineralogy and Petrology* 147, 58–73. https://doi.org/10.1007/s00410-004-0586.

Eby, G.N., 1990. The A-type granitoids: A review of their occurrence and chemical characteristics and speculations on their petrogenesis. *Lithos* 26, 115–134. https://doi.org/10.1016/0024-4937(90)90043-Z.

Eby, G.N., 1992. Chemical subdivision of the A-type granitoids: Petrogenetic and tectonic implications. *Geology* 20, 641–644. https://doi.org/10.1130/0091-7613(1992)020<0641:CSOTAT>2.3.CO;2.

El Bouseily, A.M., El Sokkary, A.A., 1975. The relation between Rb, Ba and Sr in granitic rocks. *Chemical Geology* 16, 207–219. https://doi.org/10.1016/0009-2541(75)90029-7.

Foster, M.D., 1960. *Interpretation of the Composition of Trioctahedral Micas. U.S. Geological Survey Professional Paper 354 B*. United States Government Printing Office, Washington, D.C. https://doi.org/10.3133/pp354B.

GSI, 1981. Geological map of the area adjoining the Nallamalai Fold Belt and Nellore Schist Belt, Eastern Dharwar Craton, Southern India. Geological Survey of India, Hyderabad.

Gupta, J.N., Pandey, B.K., Chabria, T., Banerjee, D.C., Jayaram, K.M.V., 1984. Rb-Sr geochronological studies on the granites of Vinukonda and Kanigiri, Prakasam district, Andhra Pradesh, India. *Precambrian Res* 26, 105–109.

https://doi.org/10.1016/03019268(84)90041X.

Haapala, I., Rämö, O.T., 1999. Rapakivi granites and related rocks: an introduction. *Precambrian Research* 95, 1–7. https://doi.org/10.1016/S0301-9268(98)00124-7.

Harris, N.B.W., Tindle, A.G., Harris, R.A., 1986. Trace element discrimination diagrams for the tectonic interpretation of granitoids. *J. Petrology* 27(4), 835–849. https://doi.org/10.1093/petrology/27.4.835.

Hazra, D., Kumar, A., David, J.S., Suresh, G., 2004. Specialised Thematic Mapping of zones of Igneous intrusive, shears and base metal mineralisation in the eastern half of the Nallamalia Fold Belt between Markapur and Karempudi, Cuddapah basin, Andhra Pradesh. *Rec. Geol. Surv. India* 136(5), 16–20.

Hokada, T., Horie, K., Satish-Kumar, M., Ueno, Y., Nasheeth, A., Mishima, K., Shiraishi, K., 2013. An appraisal of Archaean supracrustal sequences in Chitradurga Schist Belt, western Dharwar Craton, southern India. *Precambrian Res* 227, 99–119. https://doi.org/10.1016/j.precamres.2012.04.006.

Jayananda, M., Chardon, D., Peucat, J..J., Capdevila, R., 2006. 2.61 Ga potassic granites and crustal reworking in the western Dharwar craton, southern India: tectonic, geochronologic and geochemical constraints. *Precambrian Res* 150, 1–26. https://doi.org/10.1016/j.precamres.2006.05.004.

Jayananda, M., Moyen, J.F., Martin, H., Peucat, J..J., Aurvay, B., Mahabeleswar, B., 2000. Late Archaean (2550–2520 Ma) juvenile magmatism in the Eastern Dharwar craton, southern India: constraints from geochronology, Nd-Sr isotopes and whole rock geochemistry. *Precambrian Res* 99, 225–254. https://doi.org/10.1016/S03019268(99)000637.

Lameyre, J., Rocci, G., Didier, J., 1974. Granites orogéniqueset granites craton iques: reflexions sur unaspect fundamental de la geotectonique. *Geologie des Domaines Cristallins, Centenaire de la Société Géologique de Belgique, Liège* , 183–221.

Leelanandam, C., 1990. The Kandra volcanics in Andhra Pradesh: possible ophiolite? *Current Science* 59, 785–788.

Loiselle, M.C., Wones, D.R., 1979. Characteristics of Anorogenic Granites. *Geological Society of America, Abstracts with Programs* 11, 468.

Maniar, P.D., Piccoli, P.M., 1989. Tectonic discrimination of granitoids. *Geological Society of America Bulletin* 101, 635–643. https://doi.org/10.1130/0016-7606(1989)101.

Meen, J.K., Rogers, J.J.W., Fullagar, P.D., 1992. Lead isotopic compositions in the western Dharwar craton, southern India: evidence for distinct middle Archaean terrains in a late Archaean craton. *Geochim. Cosmochim. Acta* 56, 2455–2470.

Meshram, T., Lachhana Dora, M., Baswani, S.R., Ranjan, S., Nanda, J.K., 2021. Petrogenesis and U-Pb geochronology of charnockites flanking the Pranhita Godavari rift in peninsular India-link between the Bastar and Eastern Dharwar. *Gondwana Research* 92, 113–132. https://doi.org/10.1016/j.gr.2020.12.024.

Meshram, T., Mahapatro, S., Sesha Sai, V.V., Dora, M.L., Randive, K., Baswani, S., 2022. Petrogenesis of phlogopite-pyroxenite from Southern India: Implications for the link between Proterozoic subduction to rift-related arc magmatism. *Geosystems and Geoenvironment* 1, 4, 100033. https://doi.org/10.1016/j.geogeo.2022.100033.

Moyen, J.F., Nedelec, A., Martin, H., Jayananda, M., 2003. Syntectonic granite emplacement at different structural levels: the Closepet granite, South India. *J. Struct. Geol* 25, 611–631.

Mukherjee, S., Ghosh, G., Das, K., Bose, S., Hayasaka, Y., 2017. Geochronological and geochemical signatures of the granitic rocks emplaced at the north-eastern fringe of the Eastern Dharwar Craton, South India: Implications for late Archean crustal growth. *Geological Journal* 53, 1781–1801. https://doi.org/10.1002/gj.3007.

Nachit, H., Ibhi, A., Abia, E.H., 2005. Discrimination between Primary Magmatic Biotites, Reequilibrated Biotites and Neoformed Biotites. *Comptes Rendus Geoscience* 337(16), 1415–1420. https://doi.org/10.1016/j.crte.2005.09.002.

Nagaraja Rao, B.K., Ramalingaswamy, G., Rajurkar, S.T., 1987. Stratigraphy, structure and evolution of the Cuddapah basin. In Purana basins of Peninsular India. *Mem. Geol. Soc. India* (6), 33–86.

Nakamura, N., 1974. Determination of REE, Ba, Fe, Mg, Na, and K in carbonaceous and ordinary chondrites. *Geochimica et Cosmochimica Acta* 38(6), 757–775. https://doi.org/10.1016/0016-7037(74)90149-5.

Narshimha, Ch., Kumar, S., 2024. Syntectonic shear induced emplacement of crystallizing granite magmas evident from magmatic shear sense, mafic schlieren, and microgranular enclaves in the Mesoproterozoic A type Kanigiri Pluton, Nellore Schist Belt, Southeast India. *Journal of Geological Society of India* 100(5), 639 646. https://doi.org/10.17491/jgsi/2024/173886.

Narshimha, Ch., Sesha Sai, V.V., Reddy, U.V.B., Kumar, T.V., Babu, E.V.S.S.K., Sreenivas, B., Subramanyam, K.S.V., 2022. Geochemistry and new zircon U-Pb geochronology of Mesoproterozoic Punugodu granite pluton, SE India: implications for anorogenic magmatism along the western margin of Nellore Schist Belt, India. *Geological Magazine* 159, 1–21. https://doi.org/10.1017/S0016756822000073.

Pearce, J.A., Hams, N.B.W., Tindle, A.G., 1984. Trace element discrimination diagrams for the tectonic interpretation of granitic rocks. *J. Petrol* 25, 956–983. https://doi.org/10.1093/petrology/25.4.956.

Peucat, J.J., Mahabaleswar, M., Jayananda, M., 1993. Age of younger tonalitic magmatism and granulite metamorphism in the amphibolite–granulite transition zone of southern India (Krishnagiri area): comparison with older peninsular gneisses of Gorur- Hassan area. *J. Metamorph. Geol* 11, 879–888. https://doi.org/10.1111/j.1525-1314.1993.tb00197.x.

Peucat, J..J., Jayananda, M., Chardon, D., Capdevila, R., Fanning Marc, C., Paquette, J.L., 2013. The lower crust of Dharwar craton, south India: patchwork of Archean granulitic domains. *Precambrian Res* 227, 4–29. https://doi.org/10.1016/j.precamres.2012.06.009.

Pouchou, J.L., Pichoir, F., 1984. A new model for quantitative X ray microanalysis. I. Application to the analysis of homogeneous samples. *La Recherche Aérospatiale* 3, 13–38.

Powell, C.M., Pisarevsky, S.A., 2002. Late Neoproterozoic assembly of East Gondwana. *Geology* 30, 3–6.

Radhakrishna, B.P., Naqvi, S.M., 1986. Precambrian continental crust of India and its evolution. *Journal of Geology* 94(2), 145–166. https://doi.org/10.1086/629020.

Rajesh, H.M., 2000. Characterization and origin of compositionally zoned aluminous A-type granite from South India. *Geological Magazine* 137, 291–318. https://doi.org/10.1017/S001675680000399X.

Ramo, O.T., Haapala, I., 1995. One hundred years of Rapakivi Granite. *Mineralogy and Petrology* 52, 129–185. https://doi.org/10.1007/BF01163243.

Reddy, U.V.B., Naryana, B.L., Shanti Kumar, C., 1994. Ophiolite melange from Nellore Schist belt: An evidence for Precambrian plate tectonics, in: Workshop on Eastern Ghats Mobile Belt, Vishakapatnam, p. 21–22. (abs).

Rekha, S., Bhattacharya, A., 2014. Paleoproterozoic/Mesoproterozoic tectonism in the northern fringe of the Western Dharwar Craton (India): Its relevance to Gondwanaland and Columbia supercontinent reconstructions. *Tectonics* 33, 347–595. https://doi.org/10.1002/2013TC003335.

Rogers, J.J.W., Santosh, M., 2002. Configuration of Columbia, a Mesoproterozoic supercontinent. *Gondwana Research* 5, 5–22. https://doi.org/10.1016/S1342-937X(05)70883-2.

Saha, D., Mazumder, R., Kar, R., 2018. Shallow marine to pelagic sediments from a dismembered ophiolite, Kandra, southern India – Glimpses of ancient subduction zone related sedimentation. *Gondwana Research* 49, 21–41.

Sain, A., Saha, D., 2018. Structure and tectonics of a Mesoproterozoic ophiolite – Insight from Kanigiri Ophiolite with a mélange zone, southern India. *Tectonophysics* 744, 177–204. https://doi.org/10.1016/j.tecto.2018.06.017.

Sain, A., Saha, D., Joy, S., Jelsma, H., Armstrong, R., 2017. New SHRIMP age and microstructures from a deformed A type granite, Kanigiri, southern India: Constraining the hiatus between orogenic closure and postorogenic rifting. *The Journal of Geology* 125(2), 241 259. https://doi.org/10.1086/690196.

Santosh, M., Tsunogae, T., Malaviarachchi, S.P.K., Zhang, Z., Ding, H., Tang, L., Dharmapriya, P.L., 2014. Neoproterozoic crustal evolution in Sri Lanka: Insights from petrologic, geochemical and zircon U-Pb and Lu-Hf isotopic data and implications for Gondwana assembly. *Precambrian Research* 255, 1 29. https://doi.org/10.1016/j.precamres.2014.09.017.

Sesha Sai, V.V., 2013. Proterozoic Granite Magmatism along the Terrane Boundary Tectonic Zone to the East of Cuddapah basin, Andhra Pradesh - Petrotectonic Implications for Precambrian Crustal Growth in Nellore Schist Belt of Eastern Dharwar Craton. *Geological Society of India, Bangalore* 81, 167–182. https://doi.org/10.1007/s12594-013-0020-z.

Sesha Sai, V.V., 2019. Proterozoic Magnesian Feldspathic Magmatism in the Nallamalai Fold Belt, Southern India - Petrogenesis of Vellaturu-Ipuru-Nakerikallu (VIN) Arc Magmatic Granites, Eastern Dharwar Craton. *Jour. Geol. Society of India* 19(4), 409–418.

Sesha Sai, V.V., 2023. Arc-rifted arc Mesoproterozoic felsic magmatism in Nallamalai Fold Belt-Nellore Schist Belt domain; implications for Cordilleran type tectonics along eastern margin of Dharwar Craton, India. *Indian Journal of Geosciences* 77(3), 293–307.

Sheppard, S., Rasmussen, B., Jian, W.Zi, S., Sekhar.V., Sarma, D.S., Mekala, R.M., Krapež, Wilde, S., McNaughton.N.J., 2017. U-Pb dating of metamorphic monazite establishes a Pan-African age for tectonism in the Nallamalai Fold Belt, India. *Journal of the Geological Society* 174(6), 1062–1069. https://doi.org/10.1144/jgs2017-051.

Smith, J.V., Brown, W.L., 1988. Feldspar Minerals, in: Crystal Structures, Physical, Chemical, and Microtextural Properties. 2nd ed.. Springer Verlag, Berlin. volume 1.

Srinivasan, B., Radhakrishna, B.P., Naqvi, S.M., 1994. Geological Map of the Area Adjoining the North and South Nallamalai Shear Zones, Eastern Dharwar Craton, Southern India, in: Radhakrishna, B.P. (Ed.), Purana Basins of Peninsular India. Geological Society of India. volume Memoir 6, p. 33–86.

Sun, S.S., McDonough, W.F., 1989. Chemical and isotopic systematics of oceanic basalts: Implications for mantle composition and processes, in: Saunders, A.D., Norry, M.J. (Eds.), Magmatism in the Ocean Basins. Geological Society. Special Publications, London. volume 42, p. 313–345. https://doi.org/10.1144/GSL.SP.1989.042.01.19.

Swaminath, J., Ramakrishnan, M., Viswanatha, M.N., 1976. Dharwar Startigraphic model and Karnataka craton evolution Rec. *Geol. Surv. India* 107(2), 149–175.

Tatsumi, Y., Hamiliton, D.L., Nesbitt, R.W., 1986. Chemical characteristics of fluid phase released from a subducted lithosphere and origin of arc magams: evidence from high pressure experiments and natural rocks. *Journal of Volcanology and Geothermal Research* 29, 293–309. https://doi.org/10.1016/0377-0273(86)90049-1.

Upadhyay, D., 2007. Alkaline magmatism along the southeastern margin of the Indian shield: Implications for regional geodynamics and constraints on craton Eastern Ghats Belt suturing. *Precambrian Research* 162, 59–69. https://doi.org/10.1016/j.precamres.2007.07.012.

Upadhyay, D., Raith, M.M., Mezger, K., Hammerschmidt, K., 2006. Mesoproterozoic rift related alkaline magmatism at Elchuru, Prakasam Alkaline Province, SE India. *Lithos* 89, 447–477. https://doi.org/10.1016/j.lithos.2005.07.004.

Vijaya Kumar, K., Leelanandam, C., Ernst, W.G., 2011. Formation and fragmentation of the Palaeoproterozoic supercontinent Columbia: evidence from the Eastern Ghats Granulite Belt, southeast India. *Int. Geol. Rev* 53, 1297–1311. https://doi.org/10.1080/00206814.2010.527658.

Whalen, J., K, Currie, Chappell, B., 1987. A-type granites: geochemical characteristics, discrimination and petrogenesis; Contrib. *Mineral. Petrol* 95, 407–419. https://doi.org/10.1007/BF00402202.

Windley, B.F., 1995. *The Evolving Continents*. John Wiley and Sons, New York.

Zhao, G., Cawood, P.A., Wilde, S.A., Sun, M., 2002. Review of global 2.1-1.8 Ga orogens: Implications for a pre–Rodinia supercontinent. *Earth Science Reviews* 59, 125–162. https://doi.org/10.1016/S0012-8252(02)00073-9.

Zhao, G., Li, S., Sun, M., Wilde, S.A., 2011. Assembly, accretion, and break-up of the Palaeo-Mesoproterozoic Columbia supercontinent: record in the North China Craton Revisited. *Int. Geol. Rev* 53, 1331–1356. https://doi.org/10.1080/00206814.2010.527631.

Zhao, G.C., Sun, M., Wilde, S.A., Li, S.Z., 2004. A Paleo-Mesoproterozoic supercontinent: Assembly, growth and breakup. *Earth Science Reviews* 67, 91–123. https://doi.org/10.1016/j.earscirev.2004.02.003.

